Tin Oxide Electron-Selective Layers for Efficient, Stable, and Scalable Perovskite Solar Cells

DOI: 10.1002/ ((please add manuscript number))
Article type: Review

Tin oxide electron selective layers for efficient, stable, and scalable perovskite solar cells

Cesur Altinkaya[*], Erkan Aydin[*], Esma Ugur, Furkan H. Isikgor, Anand S. Subbiah, Michele De Bastiani, Jiang Liu, Aslihan Babayigit, Frédéric Laquai, Abdullah Yildiz, Stefaan De Wolf[*]

C. Altinkaya, Prof. A. Yildiz
Ankara Yıldırım Beyazıt University, Department of Energy Systems Engineering, Faculty of Engineering and Natural Sciences, Ankara 06010, Turkey
E-mail address: cesuraltnky@gmail.com;
Dr. E. Aydin, E. Ugur, Dr. F. H. Isikgor, Dr. A. S. Subbiah, Dr. M. De Bastiani, Dr. J. Liu, A. Babayigit, Prof. F. Laquai, Prof. S. De Wolf
King Abdullah University of Science and Technology (KAUST), KAUST Solar Center (KSC), Physical Sciences and Engineering Division (PSE), Thuwal 23955-6900, Kingdom of Saudi Arabia.
E-mail address: erkan.aydin@kaust.edu.sa; stefaan.dewolf@kaust.edu.sa
A. Babayigit
Hasselt University, Institute for Materials Research (IMO), Wetenschapspark 1, 3590 Diepenbeek, Limburg, Belgium.
IMEC vzw. Division IMOMEC, Wetenschapspark 1, 3590 Diepenbeek, Limburg, Belgium.

Keywords: electron selective layer; tin oxide; SnO_2; low-temperature processing; perovskite solar cells

Abstract

Perovskite solar cells (PSCs) have advanced to become a promising photovoltaic technology, where electron-selective layers (ESLs), as an integral part of the devices, have a distinctive role in such progress. To date, the mesoporous titanium dioxide (TiO_2) / compact TiO_2 stack has been among the most used ESLs in state-of-the-art PSCs. However, this material requires high-temperature sintering and may induce hysteresis under operational conditions, raising concerns about its use towards device commercialization. Recently, tin oxide (SnO_2) has emerged as an attractive alternative ESL, thanks to its favorable features such as a wide bandgap with high optical transmission, high carrier mobility, suitable band alignment with perovskites, and decent chemical stability. Additionally, its low-temperature processability enables compatibility with temperature-sensitive substrates, and thus flexible devices and tandem solar

cells. Here, the notable developments of SnO_2 as a perovskite-relevant ESL is scrutinized by emphasizing its various fabrication methods and interfacial passivation routes towards champion solar cells with high stability. Further, a techno-economic analysis of SnO_2 materials for large-scale deployment together with a processing-toxicology assessment is presented. Finally, a perspective on how SnO_2 materials can be instrumental in successful large-scale module and perovskite-based tandem solar cell manufacture is provided.

1. Introduction

PSCs have rapidly surged to be an attractive thin-film photovoltaic (PV) technology in the last decade, with power conversion efficiencies (PCEs) nowadays over 25% for single-junction devices.[1-3] This remarkable device progress is not surprising since metal-halide perovskites have excellent optoelectronic properties such as steep optical absorption edge, implying excellent semiconductor quality,[4,5] small exciton binding energy (≤10 meV),[6,7] high absorption coefficient (~10^5 cm^{-1}) in the visible and near-infrared region,[8,9] long charge-carrier lifetime (~1 µs) and diffusion length (>2 µm),[10,11] as well as a low trap-state density (10^{15}-10^{17} cm^{-3}).[12-15] The convenience of solution processing of metal-halide perovskites has rapidly lead to a widespread diffusion of PSC research across the world, which has been another contributing factor to the rapid progress of this field of research.[16]

Historically, the first examples of PSCs in solid-state form were in the *n-i-p* configuration, built on mesoporous TiO_2 (m-TiO_2) as ESL; a heritage from dye-sensitized solar cells.[17,18] Later, compact TiO_2 (c-TiO_2, a thin planar layer) was inserted underneath m-TiO_2 to prevent device shunting and increase the charge-extraction efficiency at the contacts. For a long period, the c-TiO_2/m-TiO_2 stack was a key component in many champion PSCs.[19] However, the continuous drive to push the PCE towards the 30% barrier has lately increased the search for more efficient and versatile ESLs. To date, numerous materials have already been studied to possibly replace the c-TiO_2/m-TiO_2 stack in PSCs; most of them are metal oxides such as SnO_2, ZnO, Nb_2O_5, Zn_2SnO_4, $SrTiO_3$, $BaSnO_3$, CoO_x, In_2O_3, and WO_x, but also other material systems have been evaluated such as phenyl-C_{61}-butyric acid methyl ester (PCBM), C_{60}, and CdS.[20-26] Among all these materials, SnO_2 stands out as particularly promising due to its combination of desirable features such as a wide bandgap with high optical transmittance in the visible range, high electron mobility, low conduction band (CB) offsets with commonly used perovskite absorbers, and decent chemical stability. In 2015, low-temperature processed (≤ 200 °C) SnO_2 based PSCs

were introduced by Ke *et al.*, with a champion PCE of 17.2%.[27] Following this report, the research of SnO_2 materials as efficient ESLs rapidly accelerated, with currently reported PCE values as high as 23.56%.[28] (see **Infographic 1 and Figure 1**) Following the successful demonstration of SnO_2-based PSCs on the lab-scale, the research focus is now shifting towards full exploitation of the advantages such ESL may offer compared to its more traditional TiO_2 counterpart.[29-38] For instance, low-temperature processed SnO_2 ESLs only need a post-deposition annealing temperature below ≤ 200 °C, which enables a simple, scalable and energy-efficient process,[39] with low capital investment.[40,41] Moreover, these ESLs are compatible with temperature-sensitive substrates, enabling the fabrication of flexible devices (**Figure 1**) and thus roll-to-roll manufacturing, as well as tandem devices.[42] We summarize the advantages of SnO_2 utilization in PSCs in **Infographic 2**.

In this review, we first describe the processing methods of SnO_2 ESLs for highly-efficient rigid and flexible devices, updating and extending earlier reports.[35,37,43-45] Next, following the identification of harmful defects and their origins, we scrutinize relevant defect and interfacial passivation routes for further performance enhancements and give a lab-to-fab perspective regarding their implementation in scaled device manufacturing. We complement this with a techno-economic analysis towards SnO_2 implementation for terawatt-scale PSC deployment, along with a sustainability and processing-toxicology analysis. Finally, we elucidate the key challenges in the performance-cost-stability relation that remain to be addressed and give an outlook on how such successful ESLs can be adapted for large-scale modules and perovskite-based tandem solar cell manufacturing.

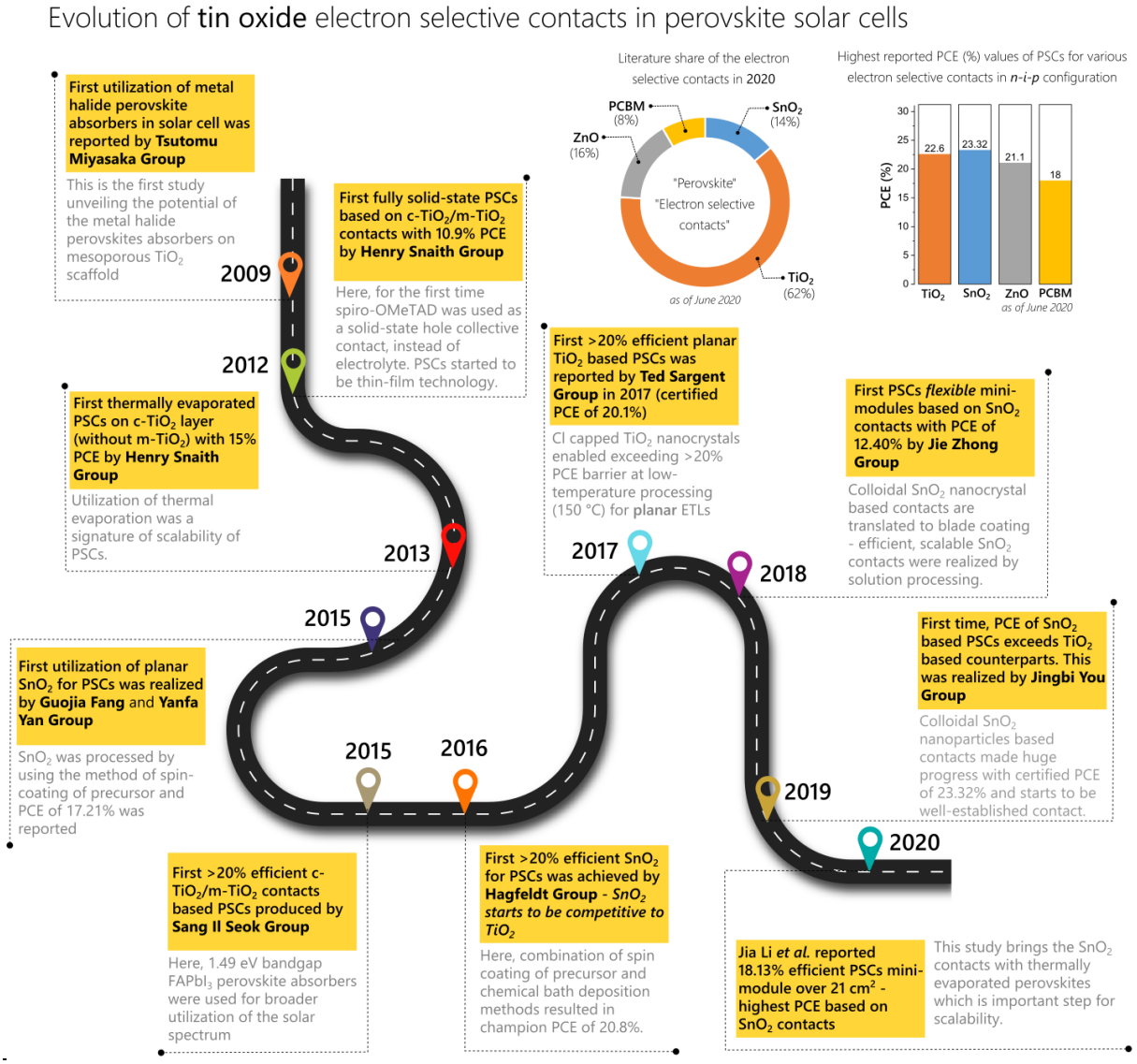

Infographic 1. Historical evolution of efficient SnO_2 contacts highlighting the important milestones together with the share of the number of publications for the most studied ESLs in the literature. The right top bar graph shows the highest PCE values for these ESLs reported as of June 2020 by searching keywords of "TiO_2, SnO_2, ZnO, PCBM and perovskite solar cells" in Web of Science database. The values represent both *n-i-p* and *p-i-n* configurations.

2. SnO_2 as an efficient electron selective layer

In PSCs, electron- and hole-selective layers (ESLs and HSLs, sometimes also referred to as *n*- and *p*-type layers, respectively) are needed to efficiently extract the photogenerated charges from the metal-halide perovskite absorbers, as sketched in **Figure 1**. If the ESL is deposited before perovskite deposition, this configuration is called *n-i-p*; the inverted architecture referred to as the *p-i-n* configuration. In case the deposition is on the glass, which will then be facing sunwards, the devices are in the so-called superstrate configuration, which is the case for most

single-junction PSCs. PSCs can also be in the substrate configuration, *e.g.,* in the case of silicon/perovskite and chalcogenide/perovskite tandem solar cells. Here, we limit the discussion to superstrate *n-i-p* PSCs, which is the most common device architecture. The precise location of the charge-selective layers (*i.e.* ESL and HSL) has several critical consequences on the device performance. For instance, the perovskite crystal quality and its morphology are primarily affected by the surface properties of the underlying charge-selective layers. Moreover, the appropriateness of a given perovskite deposition technique is dictated by the solubility of the underlying charge-selective layers against polar aprotic solvents. On device level, the light-harvesting efficiency can also be affected by the optical properties of these layers, especially those facing sunwards (*e.g.* ESL in the *n-i-p* configuration). **Table 1** gives a summarized comparison of SnO_2 with state-of-the-art ESLs,[26,37,46-49] which we discuss below in greater detail, with a focus on the *n-i-p* configuration.

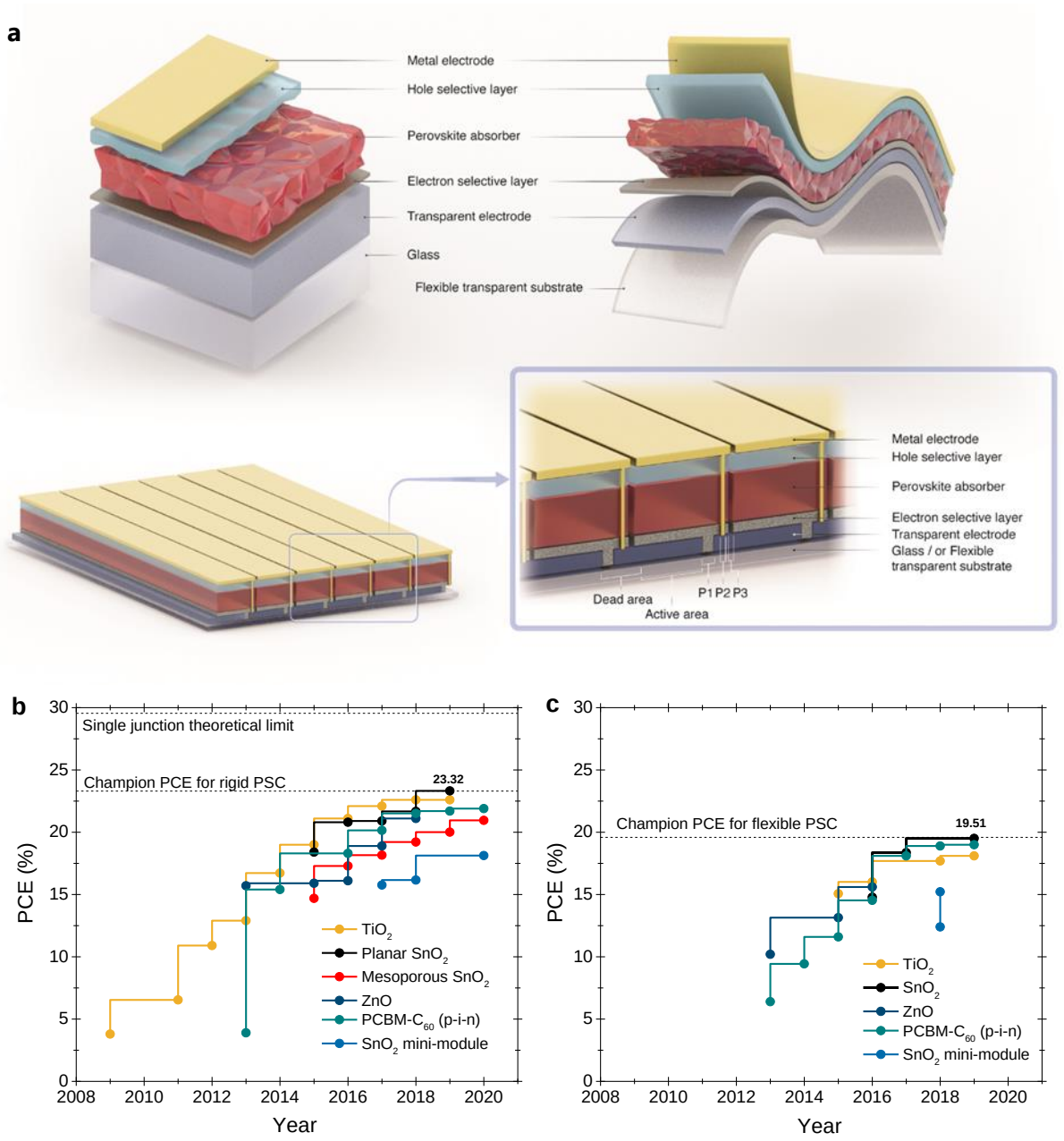

Figure 1. a) Schematics of rigid and flexible PSCs in the *n-i-p* configuration with an example of mini-modules on rigid substrates. Evolution of PCE values for b) rigid and c) flexible PSCs using state-of-the-art ESL materials. Note that for TiO_2 and SnO_2 the highest certified PCE is given for the year of 2019. Detailed PCE values are tabulated in **Table S1** and **S2**.

Large quasi-Fermi level splitting

In PSCs, a low open-circuit voltage deficit (W_{OC}, defined as $E_G/q - V_{OC}$, with E_G the bandgap, q the elementary charge, and V_{OC} the open-circuit voltage), can be considered as a measure of the high electronic quality of the bulk of perovskites, as well as the interfaces they share with the charge-selective layers. During device optimization – without the need to fabricate the full

cell stack – the absolute photoluminescence (PL) intensity of the ESL/perovskite, HSL/perovskite or ESL/perovskite/HSL stacks can be used to determine the quasi-Fermi level splitting (QFLS), which is indicative for the maximum achievable $V_{OC,\ max}$ for that device stack.[50,51] The QFLS values given in **Figure 2a** reveals that TiO_2 and SnO_2 yield higher values than typical organic ESLs such as PCBM and C_{60}, (we note that the former devices are in the *n–i–p* configuration; the PCBM based devices are in the *p–i–n* configuration).[52] This suggests that in *n–i–p* configuration devices, HSLs are voltage limiting whereas ESLs are limiting in *p–i–n* devices (without additional optimization for both selective layers) for the high V_{OC} values mainly due to the top interface quality of the perovskite. Moreover, the SnO_2/perovskite interface gives a QFLS > 1.20 eV, which is larger compared to the TiO_2/perovskite interface (1.181 eV) and close to that of the neat perovskite (1.231 eV). This implies that nonradiative recombination at the SnO_2/perovskite interface is negligible. Furthermore, although it is not included in **Figure 2a** due to the 1.60 eV bandgap selection in the graph, one of the lowest W_{OC} values (406 mV, $E_G \sim 1.62$ eV) in *n–i–p* PSCs was reported with the use of SnO_2 as ESL without any additional contact passivation.[53] Also, the record V_{OC} of 1.31 V ($E_G \sim 1.72$ eV) was obtained for SnO_2-based PSCs employing 2D perovskite top surface passivation.[54] Independent from the material characteristics, defect and contact passivation can further increase the V_{OC} (reduce the W_{OC}), which is discussed in **Section 5** in detail.[55-57]

For efficient PSCs, besides the requirement for low defect states, enabling high QFLS values, low-resistance charge transport across the device interfaces is also of critical importance. For this, ideally, the CB offset at the ESL/perovskite interface should be close to zero, else the potential barrier at the interface may hinder the efficient electron collection. Similarly, the valence band (VB) offset at the HSL/perovskite interface should be close to zero for efficient hole collection. Often, it may also be desirable to have a large VB offset at the ESL/perovskite interface to block hole transport, and a large CB offset at the HSL/perovskite interface to block

electron transport. This will aid in suppressing surface recombination of the respective interfaces, and consequently, in obtaining a large QFLS.[47,58,59] On device level, this leads to a suppression of the diode leakage current. An additional criterion for efficient charge collection is the sufficiently low (high) work function (WF) of ESLs (HSLs) compared to the perovskites, as this introduces band bending in the perovskite, aiding electrostatically in electron (hole) collection.

Figure 2c summarizes the conduction band minimum (CBM), valence band maximum (VBM), and WF values of prominent ESLs and perovskites used in high-efficiency devices. Notably, compared to other ESLs, SnO_2 has a relatively deeper CBM in reference to that of the perovskite absorber, which promotes electron extraction. Additionally, thanks to its large bandgap, the VBM of SnO_2 is much higher when compared to the other metal oxides. This suggest that SnO_2 is also more suited to block holes, and thus, suppress non-radiative recombination. Its large bandgap has additional optical benefits, which we discuss in the next sub-section.

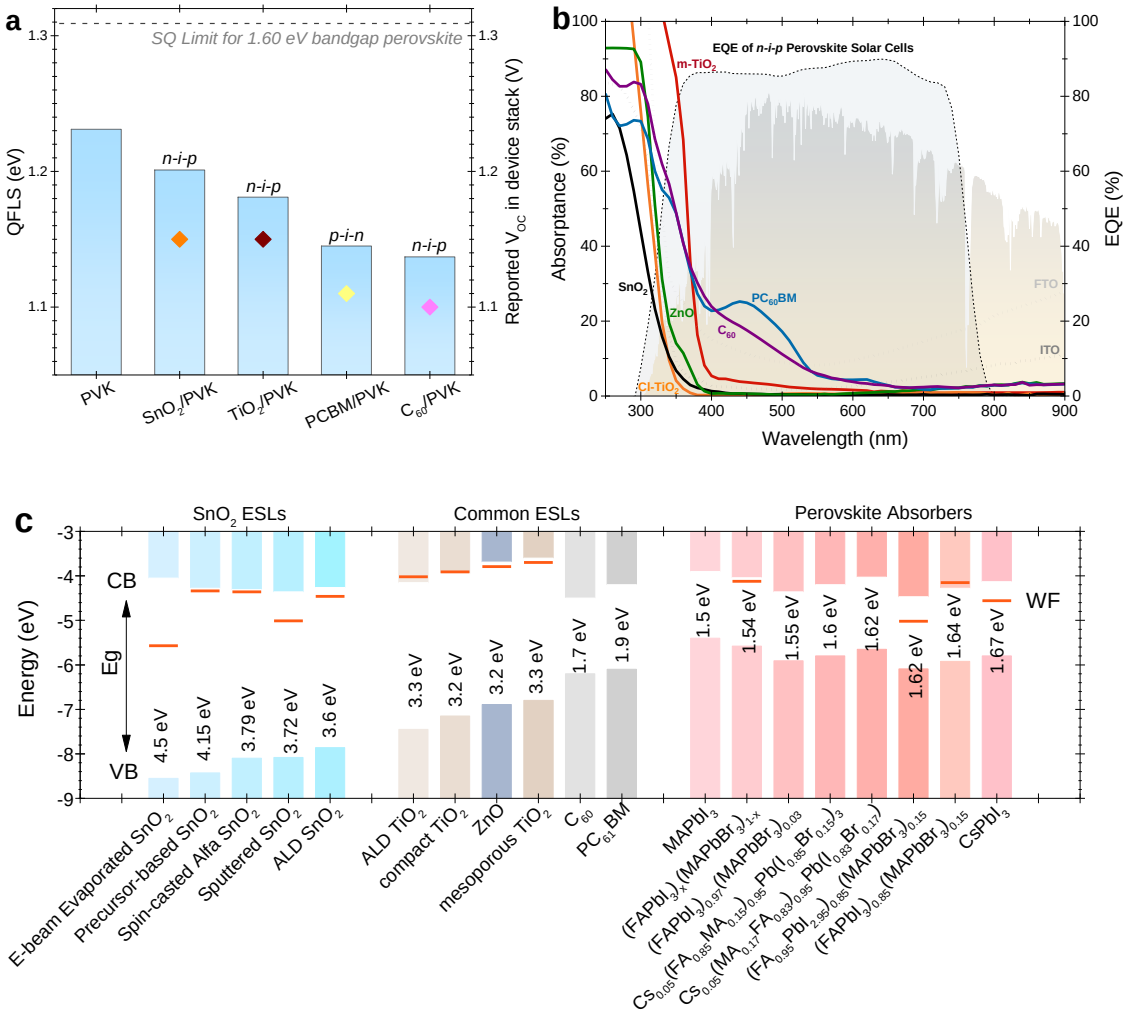

Figure 2. a) Direct comparison of QFLS values of perovskite with the various ESLs shown in gray bars. Adapted from Stolterfoht *et al.*[52], with permission from The Royal Society of Chemistry. Reported V_{OC} values from device parameters based on 1.60 eV bandgap perovskites are also included for each ESL in diamond points. (The related parameters for TiO_2,[60] SnO_2,[61] PCBM[62,63] and C_{60}[64] are taken from the literature). b) Absorptance of some state-of-the-art ESLs in literature. (Note: Absorptance spectra of FTO,[65] c-TiO_2[66] and m-TiO_2[67] are reprinted from the literature, for other ESLs in-lab experimental values were used. c) Band positions of various materials used in PSCs. Upper and lower rectangles CBM and VBM, positions, respectively; solid red line demonstrates the WF of related materials. Note, detailed parameters of band positions and corresponding references can be found in **Table S3**.

Low parasitic absorption losses

To enable a high short-circuit current density (J_{SC}) in *n-i-p* PSCs, the ESL should show a very high optical transmittance over the full solar spectrum range, particularly where its underlying perovskite layer is photoactive, *i.e.* between the bandgap range of the cover glass and perovskite (*e.g.* between ~300 – 800 nm for PSCs based on soda-lime glass and 1.55 eV perovskite). In the case of tandem devices, this range may be even larger, well beyond 1200 nm, to minimize

parasitic absorption. Actually, even in single-junction devices such broadband transparency may be required to minimize undesired device heating. **Figure 2b** shows the absorptance spectra of some common ESLs together with example EQEs of *n-i-p* PSCs with SnO_2 contacts, and **Table 1** summarizes their absorbed power which refers to which percentage of power present in sunlight is consumed by related ESLs in AM 1.5G conditions. SnO_2 features a remarkably large optical bandgap of about 3.6 – 4.5 eV, depending on its fabrication methods. Furthermore, SnO_2 possesses a relatively small refractive index (n) of ≤ 2 (at 550 nm).[68-70] Consequently, SnO_2 may improve the transmittance of fluorine-doped tin oxide (FTO) or indium-doped tin oxide (ITO) coated glass, thanks to proper refractive-index matching.[27,71] On device level, this also enables a better match with the layers in between it is sandwiched, *i.e.* the glass / transparent conductive oxide (TCO) stack[72] and the perovskite, in case of *n-i-p* PSCs, resulting in lower reflective losses. Besides, the low extinction coefficient (κ) of SnO_2 ($\kappa<0.5$, 200-1000 nm)[70,73] yields higher transparency in the ultraviolet and visible in comparison to other metal-oxide ESLs such as TiO_2 and ZnO, and organic ESLs such as PCBM and C_{60} that usually show optically a much poorer performance due to their high parasitic absorption in the blue region (**Figure 2b**).

The bandgap mainly dictates the transparency in the short-wavelength part of the spectrum. Conversely, long-wavelength transparency can be hampered by free-carrier absorption (FCA). For SnO_2 films, the carrier density can be as high as 10^{20} cm^{-3}, for which the absorption loss in the visible is still relatively weak, on the order of 0.5%. This is related to the fact that the gap between its first and second CB at the Brillouin zone center is up to 4.75eV. This ensures that even heavily doped SnO_2 has a high optical transparency, since interband direct transitions in the visible region are difficult to occur.[74] However, a high doping concentration – needed to obtain a high carrier density – results in strong interface recombination. Therefore, an optimized SnO_2 layer as ESL in PSCs usually has a much lower carrier density, generally between 10^{15}

and 10^{19} cm^{-3}, enabling the combination of a very high broadband transparency without inducing much interface recombination. The relatively low carrier concentration of state-of-the-art SnO_2 films may explain their moderate WF values, compared to other ESLs. However, these layers combine a high optical transparency with high electron selectivity, owing to their large VB offsets with perovskites, which effectively block holes. To fully exploit this transparency, the absorptance of the TCOs should be low in the range of the EQE spectra of perovskites.[65]

Low hysteresis index

PSCs can suffer from hysteresis in their current-voltage characteristics. Such behavior is undesirable as hysteretic devices deliver less stabilized power and often suffer from reduced operational stability, compared to hysteresis-free devices. The hysteresis index, defined as the relative difference in the performance between reverse (V_{OC} to J_{SC}) and forward (J_{SC} to V_{OC}) sweeping directions, can be used as a figure of merit to quantify the discrepancy between the two scanned *J-V* curves.[75] In the context of ESLs, hysteresis is mainly caused by two phenomena: (i) The presence of a large CB offset at the ESL/perovskite interface (see **Figure 2c**), causing an energetic barrier for electron extraction,[76] and (ii) a mismatch between electron and hole extraction capabilities of the contacts at opposite device ends.[77] To overcome this issue, the electron selectivity can be increased by improving the energetic alignments, utilizing high electron mobility ESLs, and enhanced charge extraction speed at the HSL side. In addition, it has also been found that for defective ESLs such as TiO_2, contact passivation can reduce surface recombination as well as hysteresis.[77,78] Considering these points, SnO_2 offers a great advantage with its low CB offsets with most perovskites, its high electron mobility (up to 421 cm^2 $(V.s)^{-1}$)[37,79] and conductivity which enhances its electron transfer capability. Combined with its low interface defect density, these advantages lead to decreased device hysteresis due to the suppressed charge accumulation at the interface between perovskite and ESL.[79,80]

Long-term operational stability

With the successful demonstration of PSCs as an efficient PV technology, a major concern towards market entrance remains the long-term operational stability of PSCs, which includes the phase stability of perovskites, contact stability, and encapsulation. From a contact stability perspective, the widely used TiO_2 contains many oxygen vacancies (or Ti^{+3} sites) at its surface that induce energetically deep trap states.[20,81,82] These trap states interact with molecular oxygen in the atmosphere by adsorption, resulting in their passivation. Under operating conditions of the device — in particular upon ultraviolet (UV) exposure (leading to interband charge excitation) — the deep trap states are reactivated by oxygen desorbing, leading to a rapid increase in recombination and hence performance loss. Also, due to its strong light-induced chemical activity, TiO_2 has the intense ability to extract electrons from organic materials which can lead to decomposition of the perovskite absorber, particularly in the presence of O_2 and H_2O.[20,83,84] In the PSC case, upon UV light illumination, electrons in the TiO_2 VB are excited into its CB, and TiO_2 can strongly extract electrons from an I^- anion in the perovskite absorber ($I^- \leftrightarrow I_2 + 2e^-$) leading to molecular iodide formation (I_2) and thus perovskite degradation. Next, ZnO was early on investigated as a promising alternative to TiO_2 due to its relatively high electron affinity and wide variety of preparation methods, which makes this a material of interest for a broad range of PV technologies.[58,85] However, due to the presence of hydroxyl groups, the basic nature of ZnO leads to deprotonation of the perovskite surface and usually causes perovskite decomposition into its precursors (*i.e.* lead iodide, PbI_2).[20,86,87]

Unlike these materials, SnO_2 is a chemically inert material with negligible catalytic properties. Due to its larger bandgap with respect to TiO_2, SnO_2 is relatively irresponsive to UV-light, making it more stable than its ESL counterparts,[88] which also paves the way for more stable PSCs. The latter was probed by tracking their maximum power point (MPP) over time,[89,90] by

1000h light soaking[91], as well as high-intensity UV light illumination [92] tests under an inert atmosphere. The stability comparison of various ESLs with SnO_2 is given in **Figure 3.**

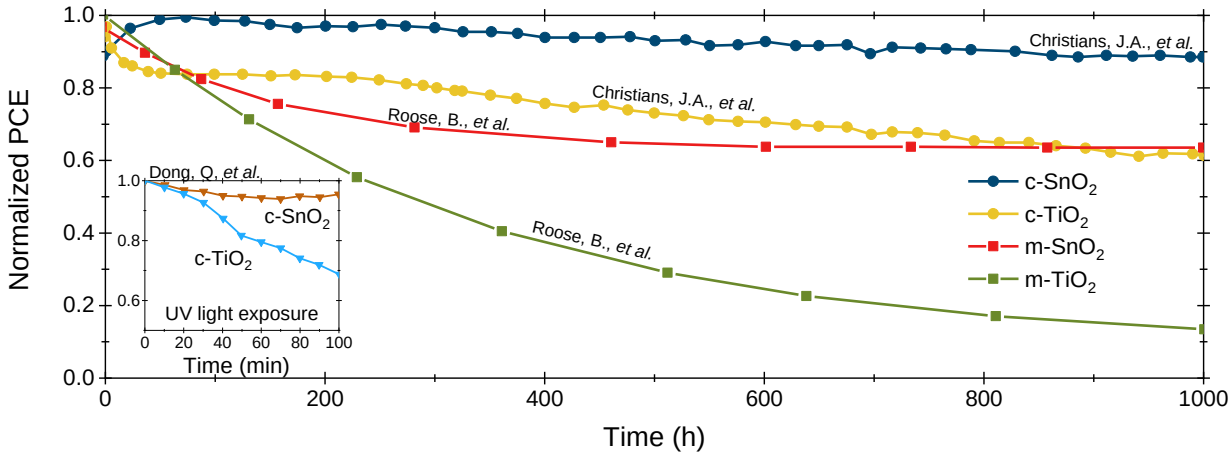

Figure 3. Stability measurements of unsealed PSCs with various ESLs under different conditions. For c-TiO_2 and c-SnO_2 ESLs, the operational stability of devices with c-ESL/FAMACs/EH44/MoO_x/Al structure under 100 mW cm^{-2} illuminations (without UV filter and following ISOS-L-1 test protocols) and ambient conditions (RH 10-20%, 26-30 °C).[90] For m-TiO_2 and m-SnO_2 ESLs, the long-term stability of devices under 100 mW cm^{-2} continuous illumination in an inert atmosphere.[91] (Inset: the stability of ESLs against intense UV irradiation of 50 mW cm^{-2} under 30% RH at 20 °C).[92]

Low-temperature processing

Notably, *m*-TiO_2, currently still the most employed ESL, usually needs high-temperature annealing at ~ 500 °C, which is needed to eliminate the organics/additives, resulting in the mesoporous structure.[93,94] SnO_2 can also be fabricated in a mesoporous structure through a similar high-temperature annealing step.[95] However, *m*-SnO_2 based PSCs have remained less efficient compared to their *m*-TiO_2 counterparts, which is mainly caused by two reasons. Firstly, high-temperature annealing leads to an agglomeration of SnO_2 nanoparticles, resulting in a non-uniform film coverage with pinholes.[79,89,95] Electronically, this agglomeration leads to a shrinking of the SnO_2 bandgap, possibly due to a reduced quantum confinement in the resulting larger particles.[79] Secondly, the crystallinity of SnO_2 improves with elevated temperature (>400 °C), which dramatically increases its free-electron density. In turn, this may inflate recombination at the ESL/perovskite interface.[79,95] Moreover, only few transparent electrodes

underneath these ESLs can withstand such sintering temperatures, with FTO as a notable exception. However, FTO significantly suffers from parasitic absorption, particularly from FCA,[65] making the FTO/ESL contact stack suboptimal for *n-i-p* device implementation. In addition, processing of ESLs at low temperature is critical towards compatibility with temperature-sensitive substrates (*e.g.*, polyethylene terephthalate, PET; polyethylene naphthalate, PEN),[96] and transparent electrodes (*e.g.*, ITO and related materials).[65] Their low-temperature processing therefore enables device fabrication on flexible substrates as well as tandem bottom cells that feature temperature-sensitive layers, such as silicon heterojunction solar cells.[97,98] An additional benefit of low-temperature ESLs is their simple and potentially fast preparation methods, which is highly desirable large-area applications. For these reasons, the low-temperature processability, combined with its excellent optoelectronic properties and stability, makes SnO_2 a promising ESL for a wide variety of scalable devices.

Cost-effectiveness, scalability, stability

The performance-cost-stability relation is of critical importance for the scalability of ESLs. Most of the inorganic materials used as ESLs naturally exist in the earth crust, some in relative abundance (discussed in detail in **Section 8**). Therefore, depending on the limited need for further purification, these materials can be relatively cheaper than their organic counterparts such as fullerene derivatives (*e.g.* C_{60} and PCBM). Organic materials have intensively been employed in inverted *p-i-n* PSCs; a heritage of organic solar cells.[99-101] Nevertheless, their cost is relatively high due to complex production methods, which may hinder their mass-production needed for industrial-scale applications.[37,47,102,103] Regarding the operational stability of PSCs, the impact of each device layer should be carefully assessed. For the perovskite itself, the precise composition of the perovskite precursor solution can play a decisive role. Most of the recent studies report a high reproducibility and phase stability thanks to the use of mixed-cation

lead mixed-halide perovskites,[104,105] when compared to the archetypical lead halide perovskite, $MAPbI_3$. Since this is a frequently reviewed topic, we will not discuss it here in detail.[78,106]

The scaling of thin-film PSCs into large-area modules necessitates a series connection of several sub-cells in a monolithic interconnection scheme (**Figure 1a**). The laser scribing process used to obtain such a series connection for conventional thin-film PV modules typically consists of three scribes, namely P1, P2, and P3. All scribes should have a minimal 'dead' area to minimize cell-to-module losses. The P1 step scribes the front TCO into strips, usually several mm wide, prior to any layer deposition. Following the front-charge-selective layer (*i.e.* ESL for *n-i-p* modules) and perovskite depositions, the P3 step scribes this film into strips without damaging the TCO underneath. Here, the relatively lower melting point of SnO_2 (1630 ^oC) in comparison to TiO_2 (1843 ^oC) and ZnO (1975 ^oC) lowers the laser-power requirement, reducing the thermal stress to the underlying TCO. Moreover, the high mobility of SnO_2 is more forgiving towards a low metal-TCO contact resistance.[107] The P2 scribe follows the deposition of the second charge selective layer (*i.e.* HSL for *n-i-p* modules), and scribes again all layers underneath but not the TCO. Following metallization, a final scribe follows.

Table 1. Direct comparison of common ESLs used in PSCs research and development.

Materials	Band gap (eV)	Absorbed Power (%) 300-900 nm (mW)	Electron mobility ($cm^2\ V^{-1}s^{-1}$)	Carrier concentration (cm^{-3})	Low Hysteresis Index	Low temp. processing	Scalability	Cost effectiveness	Stability
TiO_2	3.2-3.3[38,76]	0.95[a] 5.5[b]	0.1-4[22,108]	10^{16}~10^{17}[109]	●●○○○	●●○○○	●●●○○	●●●●●	●●●○○
SnO_2	3.6-4.5[76,110,111]	0.85	up to 421[79]	10^{15}~10^{16}[112,113]	●●●●●	●●●●●	●●●●●	●●●●●	●●●●●
ZnO	3.2-3.3[114]	2.16	200[38]	10^{17}~10^{19}[115,116]	●●●○○	●●●●●	●●●●○	●●●○○	●○○○○
Nb_2O_5	3.3-3.85[117,118]	1.44	~26[119]	~10^{12}[119]	●●○○○	●●●●●	●●●●●	●●●●○	●●●●●
$SrTiO_3$	~3.25[120,121]	n/a	5-8[120,122]	1×10^{17}~2.5×10^{19}[123]	●○○○○	●●●○○	●●●○○	●●●●○	●●●○○
$PC_{61}BM$	1.9[124]	9.22	$6.1\times10-2$[125]	6.6×10^{17}[126]	●●●●●	●●●●●	●●●○○	●○○○○	●●○○○
C_{60}	1.7[20]	10.45	1.6[125]	4×10^{15}[127]	●●●●●	●●●●●	●●●●○	●○○○○	●●○○○

[a] c-TiO_2; [b] c-TiO_2/m-TiO_2 stack

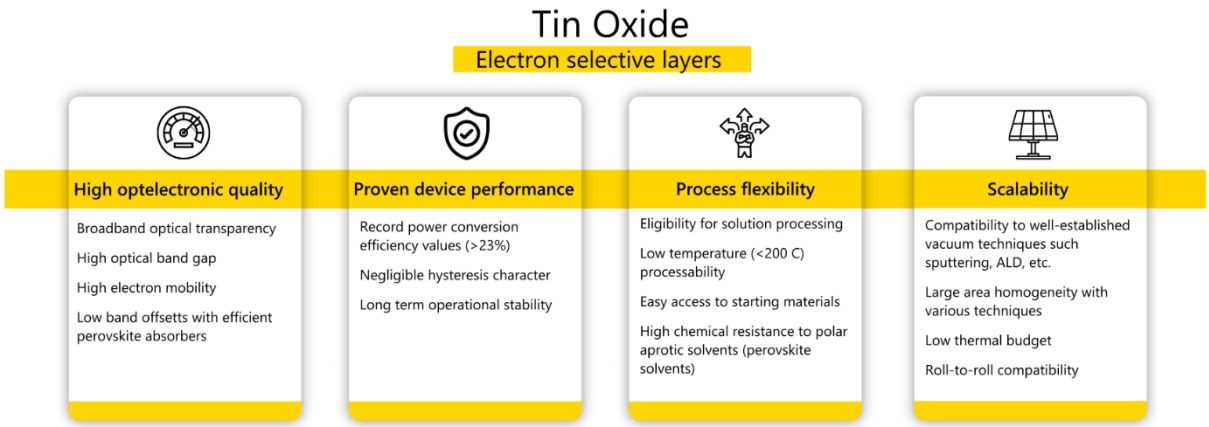

Infographic 2. Some unique properties of SnO_2 ESLs for PSCs.

3. The processing – performance relation of SnO_2 ESLs

The fabrication of SnO_2 as efficient ESL can be divided into two main classes: (i) solution processing, using precursor solutions and colloidal dispersions for deposition, and (ii) vapor deposition techniques, employing solid or liquid precursors, or target materials. Below, we discuss the advantages and drawbacks of the specific processing methods. The PCE values of some state of the art monolithic PSCs (both on flexible and rigid substrates) and the schematic illustration of various processing methods for SnO_2 ESLs can be found in **Figure 4** and **5**, respectively. Since we specifically focus on SnO_2 processing, for the scalable processing of perovskite absorbers, we also encourage readers to consult previously published reviews by Li *et al.* [128], Kim *et al.*[129] and Park *et al.*[130]

Table 2. A direct comparison of the deposition techniques of SnO_2 layers.

	Performance on PSCs	Low-temperature deposition	Conformity	Scalability	Reproducibility	Processing Speed	Cost-effectiveness
Spin-coating of precursor	●●●●○	●●●●○	●○○○○	●●○○○	●●●●○	●●●●○	●●●○○
Spin-coating of colloidal NP	●●●●●	●●●●●	●○○○○	●●●○○	●●●●○	●●●●●	●●●○○
Slot-die/blade coating of colloidal NP	●●●●○	●●●●●	●○○○○	●●●●●	●●●●●	●●●●●	●●●●○
Spray coating of colloidal NP	●●●●○	●●●●○	●●●●○	●●●●●	●●●○○	●●●○○	●●●●●
Chemical bath deposition	●●●●○	●●●●○	●●●○○	●●●●○	●●●●○	●●○○○	●●○○○
Atomic layer deposition	●●●●○	●●●●●	●●●●●	●●●●●	●●●●●	●○○○○	●●○○○
Magnetron sputtering	●●●●○	●●●●○	●●●●○	●●●●●	●●●●●	●●●○○	●●●○○
Pulsed laser deposition	●●●○○	●●○○○	●●●●○	●●●●○	●●●●●	●●○○○	●●●○○
Thermal evaporation	●●●○○	●●●●○	●●●●○	●●●●○	●●●●●	●●●●○	●●○○○
E-beam evaporation	●●●○○	●●●●○	●●●●○	●●●●○	●●●●○	●●●○○	●●●●○
Plasma treatment	●●●●○	●●●●●	●●●●●	●●●●○	●●●●○	●●●●○	●●●●○

3.1. Solution-processed SnO_2 layers

Spin-coating of precursor solutions

Spin-coating can be considered to be a medium-size area technique (areas up to a few 100 cm^2) if the homogeneity can be carefully controlled. This is a typical sol-gel process, wherein a mixture of tin chloride ($SnCl_2 \times H_2O$, a typical starting chemical) forms a solution in common solvents (*i.e.*, ethanol, isopropanol, deionized water). This solution is then cast on the TCO/glass substrate at a specific concentration, volume, and spin-speed to adjust the film thickness. Following spin-coating, the substrates are typically annealed at 180 °C, during which the film shrinks to form a metal-oxygen-metal framework. During the annealing process, residual $SnCl_2$ and other organic contaminants are removed, leading to film densification.[131] Using this method, Ke *et al.* reported the first use of SnO_2 as ESL for PSCs with PCE of 17.21%.[27] Later on, other teams reported 19.5%[53] 20.23%[132] and 20.06%[133]. To eliminate the annealing step at 180 °C, and speed-up the fabrication process, an N_2 plasma can be used. The plasma breaks the alkoxy and hydroxyl groups, and enables the formation of Sn-O-Sn networks, at room temperature, leading to PCE of 20.3%.[134] On the other hand, large-area

devices were demonstrated with precursor technique by *Li et al.*, achieving PCEs of 19.91% (maximum 20.28%), 18.97%, and 16.59% for active areas of 0.16, 1.00, and 4.00 cm^2, respectively (see **Figure 4a**).[135] Mini-modules achieved a record PCE of 18.13% for 21 cm^2 active areas (6-series connected cells, **Figure 4a** and **c**) with a decent shelf stability, retaining 95% of its initial efficiency for 60 days under a controlled environment with a humidity of 30% .[135] These examples demonstrate the applicability of SnO_2 for large-area devices with good performance.

Spin-coating of colloidal nanoparticles

Spin-coating of SnO_2 nanoparticles is the most reported protocol due to its convenience, ease of access to raw materials, and high reproducibility. This requires pre-synthesis of dispersions that are composed of nanoparticles (NPs), nanocrystals (NCs), or quantum dots (QDs), which are often commercially available at low cost, making this a promising option. In this technique, a colloidal SnO_2 dispersion (col-SnO_2) is deposited on TCO/glass substrates by spin-coating and subsequently annealed at low temperatures (typically at 150 °C to evaporate the residual water). The thickness of the films is controlled by the concentration of the solution and spin cycles. Jiang *et al.*, reported the first example of this approach in 2017 with a certified PCE of 19.9% utilizing a commercially available (Alfa Aesar) NP-based solution.[136] Later, Bu *et al.* revealed that a key to this performance is the residual K-doping effect of the SnO_2 NPs, resulting from its synthesis.[41] Subsequently, Han *et al.* scaled this technique to mini-modules,[137] by using cationic poly(allylamine hydrochloride) (PAH) polyelectrolyte on negatively charged FTO substrates to deposit SnO_2 uniformly over a large area (**Figure 4b**). In the next step, the pH of SnO_2 dispersion was adjusted to 11 (more alkaline) to charge the SnO_2 NCs negatively. Based on the electrostatic attraction formed between layers, 25 and 100 cm^2 mini-modules were fabricated with PCEs of 15.03 and 14%, respectively. Recently, 22.4 cm^2 mini-modules (7 sub

cells) with such ESL reached PCEs of 16.6% with 2000 h operational stability under 1-sun illumination by preserving 86% of its initial PCE.[138] Nevertheless, adopting this spin-coating based technique for substrates larger than 100 cm^2 is still challenging due to the high material waste (~90%), inhomogeneous deposition on substrate corners, and difficulty to deposit on curved (non-flat) substrates.[139] Fortunately, these drawbacks can be resolved by other scalable techniques such as slot-die or spray coatings, as will be discussed below.

Slot-die and blade coating of colloidal nanoparticles

Slot-die coating is a proven method for a large-area thin-film deposition since this method enables uniform deposition of films with high yield, reproducibility, and adjustable film thickness.[128] Moreover, this technique is compatible with roll-to-roll fabrication.[139] Basically, in this technique, the SnO_2 "ink" is precisely delivered onto a linearly moving substrate through slot-die head, with continuous ink supply.[41] By utilizing slot-die coating to deposit the SnO_2 layer, PSCs with moderate PCEs close to 18% and 12% for small-area devices and mini-modules have been reported, respectively.[140,141] Gao *et al.*[142] built PSCs with a PCE over 17% and Di Giacomo *et al.*[143] scaled this method up for mini modules (aperture area of 144 cm^2) with a PCE of 13.8%. At present, rather than the incapability of slot-die processed SnO_2 ESLs, the main reason behind this PCE gap between small and large area devices is arguably the lack of efficient, low-cost, and large-area HTL processing onto the perovskite layer. Reports on flexible substrates using this ink configuration are described in detail in **Section 6.** Blade coating can be considered to be a predecessor to slot-die technology, without continuous ink supply. This is an alternative method to scale-up PSCs and ESL deposition,[144,145] where colloidal SnO_2 inks have been tested as well. Peng *et al.*[146] and Dou *et al.*[147] reported small area ($\leq$ 0.15 cm^2) PSCs using blade-coated SnO_2 ESLs with PCEs of 17% and 19.6%, respectively (for detailed parameters and explanation, see **Table 4**). Despite these promising

performances achieved for small scale devices, the absence of continuous ink supply casts doubts on whether this method is suited for true scale-up.

Spray coating of colloidal nanoparticles

Spray coating is another industrially viable deposition route, combining a high fabrication speed and a relatively low material consumption with high conformality.[148-150] In this method, the precursor solution is transformed into fine liquid droplets which are dispersed onto substrates using a spray nozzle. Here, to achieve high-quality films, the ink should provide good wetting on the substrate with high uniformity, and the solvent should evaporate homogeneously.[151] Large-area perovskite mini-modules based on SnO_2 ESLs, processed via automated spray coating tools, were demonstrated by several groups as listed in **Table 4**. Here, using very short (1-min) hot air blowing, rather than longer post-annealing, can be essential to obtain the full benefits of this technique for fast fabrication.[152]

As a related technique, spray pyrolysis can also be used for the deposition of SnO_2, where chemical reactions occur on the substrate, in contrast to the use of pre-synthesized inks in the case of spray deposition. However, the formation of metal oxides on the surface of the hot substrate, during which solvent is usually instantly vaporized, often results in inadequate coverage of the material, which in turn makes the device fabrication process challenging. This may explain why there is to date no report on this technique for PSC fabrication, although thin-film deposition was demonstrated.[153-155]

Chemical bath deposition

Chemical bath deposition (CBD) for film formation is governed by two critical steps, namely nucleation and particle growth. Here, a $SnCl_2$ solution is prepared in deionized water with additives of urea and a certain fraction of acids, such as mercaptoic acid and HCl, acting as a binder and stabilizer, respectively. Then, the TCO/glass substrates are dipped into this solution.

Here, as Sn has two oxidation states, Sn^{2+} and Sn^{4+}, both ions can be found in the $SnCl_2$ solution. According to Sn^{2+}, the nucleation mechanism of forming SnO_2 could occur as follows;[131,156-158]

$$Sn^{2+} + 2OH^- \rightarrow Sn(OH)_2 \quad (1)$$
$$Sn(OH)_2 \rightarrow SnO + H_2O \quad (2)$$
$$SnO \rightarrow SnO_2 \quad (3)$$

in which $Sn(OH)_2$ (or $Sn(OH)_4$ for Sn^{4+}) precipitates on the substrate, resulting in SnO_2 nucleation. Time and temperature are the main parameters that control the SnO_2 thin-film growth and its thickness. After this process, the substrates are annealed typically at ~180 °C. In 2016, Anaraki *et al*. introduced this technique for PSC fabrication, with PCE values comparable with c-TiO_2 based devices,[53] which was also employed by other groups.[159,160] The key to these results was the utilization of a spin-casted SnO_2 compact layer underneath of the CBD layer, which works as a nucleation layer and forms denser films. The compact layer prevents shunts and consequently increases the fill factor (*FF*) of the devices. Following this, Bu *et al.* recently achieved a PCE of 20.56% for small-area devices (0.16 cm^2) and 15.76% for mini-modules (active area of 20 cm^2, six sub-cells).[161] Although CBD is a simple and inexpensive technique, the necessity of frequent bath replacement and large amount of solution waste are key challenges that may hinder its utilization for large-scale fabrication.

3.2. Vapor processed SnO_2 layers

Atomic layer deposition

To fabricate high-quality SnO_2 films, atomic layer deposition (ALD), which is based on sequential binary self-limited reactions, is frequently used.[162,163] The inherent self-limited nature of the ALD process can provide high uniformity and conformality over large areas and rough/complex surfaces, with precise control over the thicknesses down to the monolayer level. Additionally, high-quality films can be prepared at low temperatures due to the highly reactive nature of ALD precursors. In 2015, Correa-Baena *et al.* reported the first ALD deposited SnO_2

ESLs for PSCs with a PCE of 18.4%, which outperformed their ALD and solution-processed TiO_2 reference devices.[76] In 2017 the same team reached PCE >20% with a relatively high V_{OC} of 1.23 V.[164] In some cases, processing at low temperatures (<120 °C) can provide additional passivation effects as the unreacted precursor, tetrakis(dimethylamino)tin(IV) (TDMASn), partially remains in SnO_2 film.[165] The high conformality of the ALD technique also enables coating of SnO_2 layers on rough surfaces such as FTO coated glass.[166] The major limitations of the ALD technique are the relatively low processing speed and gaseous and corrosive by-products, which at times leads to substrate poisoning. Additionally, low-temperature processing usually results in amorphous films, requiring post-annealing steps to achieve poly-crystalline, conductive films. However, careful reactant choices can overcome these issues easily.

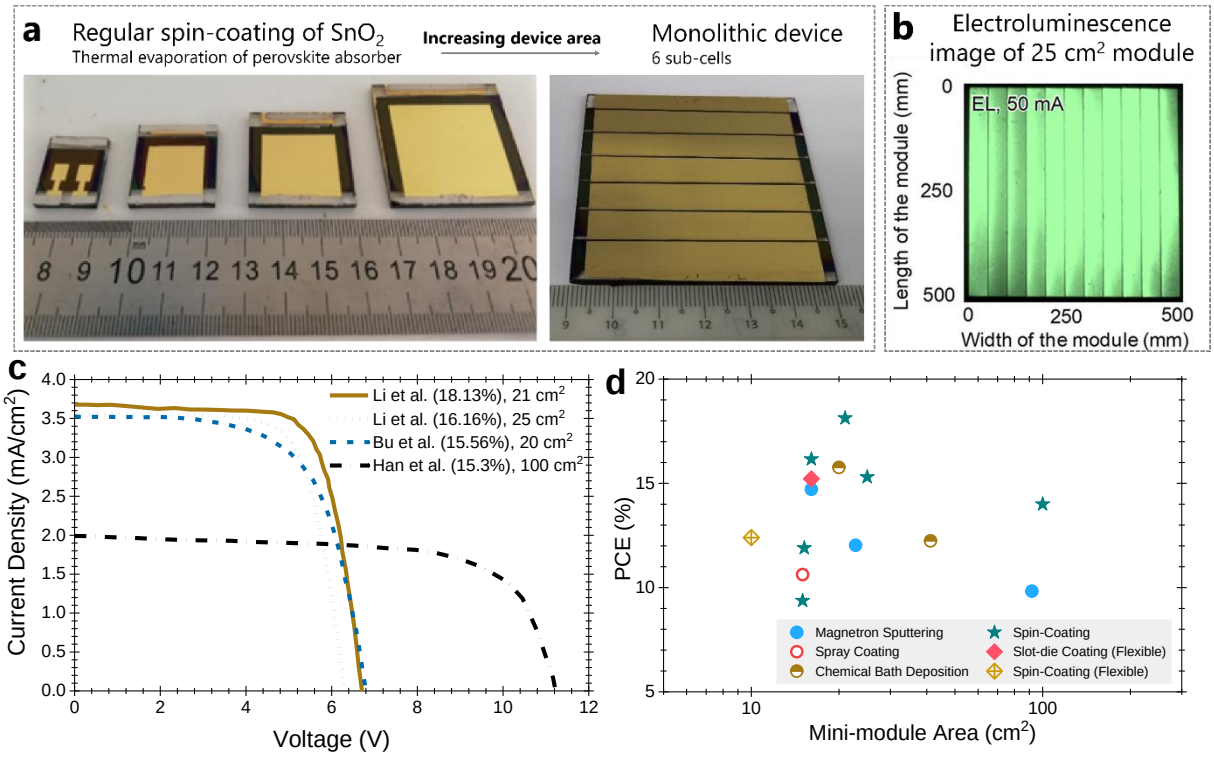

Figure 4. a) Photograph of the some PSCs with single-junction cells and 6-sub cell mini-modules using SnO_2 ESLs. Reproduced with permission.[135] Copyright 2020, Elsevier. b) Electroluminescence of the mini-modules showing minimized shunt defects via electrostatic self-assembly spin-casted SnO_2 contacts. Reproduced with permission.[137] Copyright 2019, American Chemical Society. C) Compiled J-V curves of some state-of-the art mini-modules using SnO_2 ESLs.[135,137,161,167] d) Summary of the state-of-the-art PCE values of monolithic

PSCs with SnO_2 ESLs fabricated on rigid and flexible substrates. The examples in panel d were taken from Table 4.

Magnetron sputtering

Magnetron sputtering is a mature and reliable technique for lab- and industrial-scale fabrication of metal-oxide ESLs and thin films due to its distinct advantages such as high quality and uniform deposition, strong adhesion between film layers, fine control of film density and thickness, high deposition yield, and low operational cost.[168-170] Despite these advantages, sputtering has been rarely studied so far for SnO_2 processing for PSCs, and only one study reported PCEs values >20% for a 0.09 cm^2 cell.[171] The authors also reported a PCE of 12.03% for mini-modules (aperture area of 22.8 cm^2). Following this, Bai *et al.* recently reported sputtered SnO_2 ESLs at room temperature for mini-modules (again with an active area of 22.8 cm^2) with a champion PCE of 14.71%.[94] The main challenge for the sputtering method is control of oxygen vacancies in the SnO_2 film, which is usually accomplished by tuning the gas flows during processing or post-annealing. Another concern is the amorphous or nanocrystalline nature of the films, causing band tail states, which may result in V_{OC} losses.[171] To overcome this issue, interfacial passivation routes can be applied as will be discussed in **Section 5.**

Pulsed laser deposition

Pulsed laser deposition (PLD) requires the utilization of focused laser pulses onto a given target material, resulting in a supersonic jet of ablated species that condense on the substrate. Parameters such as target concentration, substrate temperature, laser power, and oxygen pressure in the chamber control the SnO_2 film quality and its growth rate.[172,173] Even though PLD is widely studied in research laboratories, the technique is only slowly emerging for industrial applications. To achieve large-area uniformity, either the laser spot is scanned across

the target surface, or the substrate is moved during deposition. With challenges such as particle incorporation, inhomogeneous energy distribution, differences in expansion velocities of elements, and unwarranted temperature effects, not many reports have used this technique towards PSC fabrication yet; only one study demonstrated with 17.29% PCE on glass and 14% on flexible substrates.[174] However, this conceptually simple and versatile technique, even suitable for perovskite deposition,[175] may be cost-effective and suitable for large volume productions, opening new avenues for research.

Thermal evaporation

Thermal evaporation is a relatively simple and widely used technique for the homogenous fabrication of many thin-film materials with directional coverage and accurate control of thicknesses. However, the energy-intensive evaporation of SnO_2 by this technique is often challenging since the melting point of SnO_2 is relatively high (1630 ^oC).[176,177] Besides, usually a relatively high vacuum is needed. Although there have been some attempts, evaporated amorphous SnO_2 films offer almost negligible device performance due to the poor density of the films, so far. However, post-annealing of the films allowed for an instantaneous amorphous to crystalline transition with far better charge extraction and transport properties, leading to 16.8% efficient PSCs.[178] Even though not many reports have employed this technique, proper optimization and control may allow scalable fabrication of SnO_2 using thermal evaporation.

E-beam evaporation

E-beam evaporation is a related high vacuum process that delivers higher density films (compared to thermal evaporation) coatings and a high material utilization efficiency. Essentially, the target material is bombarded with an electron beam carrying sufficient energy to convert it into a gaseous phase, which is then deposited on the substrates. With this method,

large areas can be covered simultaneously. In 2017, a first example using e-beam evaporated SnO_2 was reported with 18.2% PCE values with excellent shelf stability, keeping 97% of its initial PCE over 34 days.[179] Even though this value was improved later to 18.95%,[111] this method is yet to be adapted for perovskite module fabrication. Even though the e-beam technique offers relatively high deposition rates, it is generally difficult to control the film composition precisely. Also, the X-ray damage (*bremsstrahlung*) on substrates and low processing speeds due to the need of a high vacuum are drawbacks for this technique.

In-situ plasma etching of FTO

This approach was first reported by Sun *et al*.[180] where *in-situ* SnO_2 layers are formed on the commercial FTO substrates via oxygen plasma (to remove F) without employing any Sn-based precursor or post-treatment step. Such *in-situ* SnO_2 contacts led to a champion PCE of 20.39% with remarkable stability up to 1000 h under ambient conditions (70% RH). This technique seems promising towards scaling-up of cost-efficient PSCs without additional material requirements. However, the associated rise in substrate temperature and inherent damage to the conductivity of the FTO layer can adversely affect the transport properties of the TCO. Also, F diffusion through this layer during long operational conditions may be a concern and needs to be studied separately to gauge the true potential of this technique. Finally, this approach requires the presence of FTO as a transparent electrode, which unfortunately has sub-optimal performance for high-efficiency devices due to its high parasitic absorption.

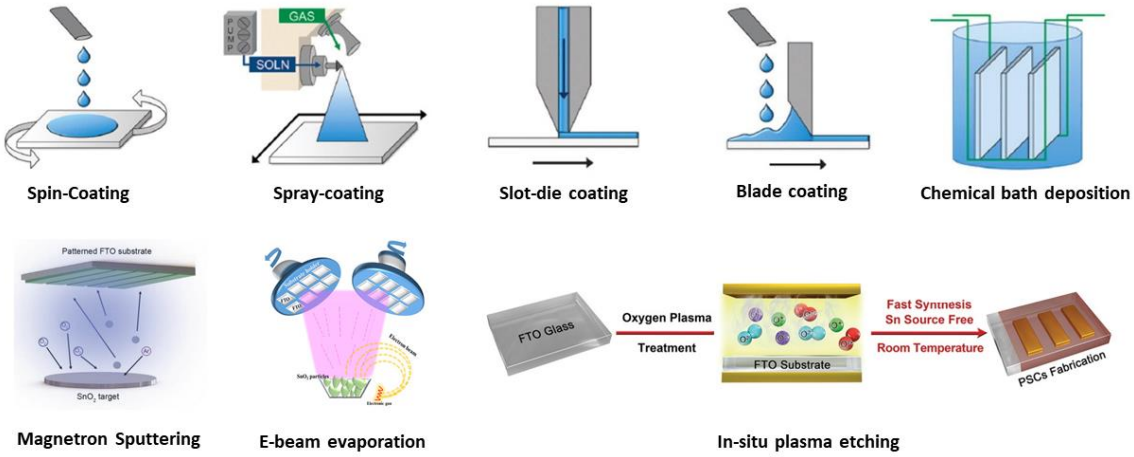

Figure 5. Illustration of various deposition methods for SnO_2 ESLs. Reproduced with permission.[171,179-181] Copyright 2016, Taylor and Francis; Copyright 2017, 2018, 2019, Wiley-VCH.

Table 3. Survey of fabrication methods for PSCs using SnO_2 ESLs. The precursors, sintering temperatures, crystallinity, device structure, and PCE are also included.

Method	Precursor	T [°C]	Crystallinity	ESL Thickness [nm]	Device Structure	PCE [%]	Stabilized PCE [%]	Ref.
Precursor-based synthesis								
SC[a]	$SnCl_2.2H_2O$	180		25	ITO/SnO_2/perovskite/spiro/Ag	20.06		[133]
SC-CBD	$SnCl_2.2H_2O$	180			FTO/SnO_2/perovskite/spiro/Au	21.20	21.01	[160]
CBD[b]	$SnCl_2.2H_2O$	180			FTO/SnO_2/perovskite/oxo-Graphene/spiro/Au	21.1	20.2	[159]
SC	$SnCl_2.2H_2O$	180		30	FTO/SnO_2/perovskite/spiro/Au	20.23	19.1	[182]
Colloidal dispersion-based synthesis								
SC	SnO_2 QDs	200	Crystalline	30	FTO/SnO_2/perovskite/spiro/Au	20.79	20.32	[113]
SC	SnO_2 NCs	130	Crystalline	40	FTO/SnO_2/$MAPbI_3$/spiro/Ag	20.52	19.62	[183]
UVO[c]-SC	SnO_2 NPs	50	Crystalline	70-100	FTO/SnO_2/perovskite/spiro/Au	20.5	20.1	[184]
SC	Alfa SnO_2	150			ITO/SnO_2/perovskite/PEAI/spiro/Au	23.56	23.32	[28]
Blade-coating	Alfa SnO_2	100			ITO/SnO_2/perovskite/spiro/Au	19.6	18.2	[147]
Spray-coating	Alfa SnO_2	120		38	ITO/SnO_2/perovskite/spiro/Au	19.2		[152]
Vapor deposition								
ALD[d]	TDMASn	118			FTO/SnO_2/PCBM:PMMA/perovskite/PMMA/spiro/Au	20.44	20.35	[185]
PEALD[e]	TDMASn	100	Amorphous	<50	FTO/SnO_2/C_{60}-SAM/perovskite/spiro/Au	20.42	20.3	[186]
Sputtering	SnO_2	RT	Amorphous	17	FTO/SnO_2/ perovskite /spiro/Au	20.2	19.8	[171]
Plasma treatment	FTO	RT	Crystalline	<8.5	FTO/SnO_2/ $MAPbI_3$ /spiro/Au	20.39	~19.88	[180]
PLD[f]	SnO_2	RT	Amorphous	8	FTO/SnO_2/PCBM/perovskite /spiro/Au	17.29	16.7	[174]
TE[g]	SnO_2	100	Crystalline		FTO/SnO_2/perovskite /spiro/Ag	16.79	15.05	[178]
E-beam Evaporation	SnO_2	200	Crystalline	50	FTO/SnO_2/ perovskite /spiro/Au	18.95		[111]

[a]Spin-coating; [b]chemical bath deposition [c]UV-Ozone treatment; [d]atomic-layer deposition; [e]plasma-enhanced ALD; [f]pulsed-laser deposition; [g]thermal evaporation

Table 4: Reported perovskite sub-modules using SnO_2 ESLs and their related parameters.

Mini-module Architecture	ESL (SnO_2) fabrication technique	Sintering Temperature [°]	Active Area [cm^2]	Total area (cm^2) Lateral Dimensions [cm×cm]	Number of cell interconnected	PCE [%]	Stability	Ref
Rigid Modules								
FTO/SnO_2/C_{60}/perovskite/spiro/Au	Sputtering		91.8[da]	100 [10×10]	14	9.83	80%, 500 h, RT[b], 1-sun, steady output	[187]
FTO/SnO_2/perovskite/spiro/Au	Sputtering	RT	22.8[aa]	25 [5×5]	6	12.03	80%, 515 h, RT, 1-sun, steady output	[171]
FTO/SnO_2/perovskite/spiro/Au	Sputtering	RT	16.07[aa]	30 [5×6]	6	14.71		[94]
FTO/SnO_2/perovskite/spiro/Au	Spray Coating	40	15	25 [5×5]	8	10.62		[188]
FTO/SnO_2/perovskite/spiro/Au	CBD	180	20	36 [6×6]	6	15.76		[161]
FTO/SnO_2/perovskite/spiro/Au	CBD	70	41.25	64 [8×8]		12.24	>80%, 200 h, 60 °C, N_2	[189]
FTO/SnO_2/perovskite/spiro/Au	Spin Coating of NPs	100	15	25 [5×5]	8	9.37		[188]
FTO/SnO_2/perovskite/spiro/Au	Spin Coating of Precursor	180	16.07[aa]	25 [5×5]	6	16.16		[167]
FTO/PAH[a]/SnO_2/perovskite/spiro/Au	Spin Coating of CNPs	150	25[da]	42.25 [6.5×6.5]	11	15.3		[137]
FTO/PAH[a]/SnO_2/perovskite/spiro/Au	Spin Coating of NPs	150	100[da]	100 [10×10]	20	14		[137]
FTO/SnO_2/perovskite/spiro/Au	Spin Coating of Precursor	180	21	36 [6×6]	6	18.13	>85%, 8000 s, MPT[c], 1-sun, 70% RH	[135]
FTO/SnO_2/perovskite/spiro/Au	Spin Coating of Precursor	180	15.2[aa]	25 [5×5]	5	11.9		[190]
ITO/SnO_2/perovskite/spiro/P3HT/Au	Spin Coating of NPs	150	22.4[da]	25 [5×5]	7	16.6	86%, 2000 h, 1-sun, operational stability	[138]
Flexible Modules								
FTO/SnO_2/perovskite/spiro/Au	Slot-die Coating	140	16.07[aa]	30 [5×6]	6	15.22	80%, 1000 h, dark, RT, 20% RH	[41]
FTO/SnO_2/perovskite/spiro/Au	Spin Coating of NPs	120	10[aa]	25 [5×5]	6	12.40		[102]

[a)]PAH: poly(allylamine hydrochloride); [b)]room-temperature; [c)]maximum power-point tracking; [aa)]aperture area; [da)]designated area (active area + dead area)

4. Defect chemistry of SnO_2

In general, SnO_2 possesses a rutile phase (*$P4_2$ / mnm*, stable at room temperature) and is a particular semiconductor among group IV oxides as it combines a high conductivity with a high visible-light transparency. SnO_2 owes these characteristics to its unique band structure and defect chemistry.[191-194] To further improve its charge selectivity, further deciphering its defect chemistry is critical, which is particularly important to define adequate passivation strategies, which is discussed in **Section 5**.

Intrinsically, SnO_2 prefers to exist in its stoichiometric composition. It can be doped to different conductivity levels, depending on the concentration of intrinsic defects and extrinsic doping

conditions. SnO_2 crystals may feature oxygen and tin vacancies (V_O, V_{Sn}), interstitials (O_i, Sn_i), as well as antisite defects (Sn_O, O_{Sn}), as sketched in **Figure 6**. Oxygen vacancies are the most typical charge states in SnO_2, together with Sn_i.[74,195] Among these, Kilic *et al.* found that Sn_i may play a more prominent role since its formation energy is much lower than that of V_O.[74] Both defects are critical for the electrical properties of the films, and form a shallow donor level near the CB, giving the *n*-type character to SnO_2 films.

Typically, these defect states occur naturally during processing. For the formation of V_O, the oxygen vapor pressure (independent from the deposition technique) and temperature are two critical parameters. This formation can be represented by $O^{-2} \leftrightarrows ½\ O_2 \uparrow + V_o^{\cdot\cdot} + 2e^-$.[195] In intrinsic SnO_2, V_O is compensated through Sn reduction ($Sn^{4+} + 2e^- > Sn^{2+}$).[196] On the other hand, extrinsic atoms (as reported in **Figure 6**) can also be used for doping SnO_2 films. From a device perspective, these unavoidable charge-trap states exist at the bulk and interface between ESL and perovskite layer and result in nonradiative recombination and deterioration of the charge extraction process.[197] In addition, severe device hysteresis occurs due to ion migration and accumulation arising from the poor interfacial contact and defects at the interface. Also, the energy band offset between SnO_2 and absorber layer may lead to a decrease in V_{OC} in some cases.[198] Therefore, passivating such defects is key to achieve champion-V_{OC} devices where two main phenomena, electron extraction and injection, take place.[199] In this direction, there are two main strategies followed in the literature (i) elemental doping, (ii) surface passivation. The following chapters discuss successful passivation routes that have been reported in literature thoroughly.

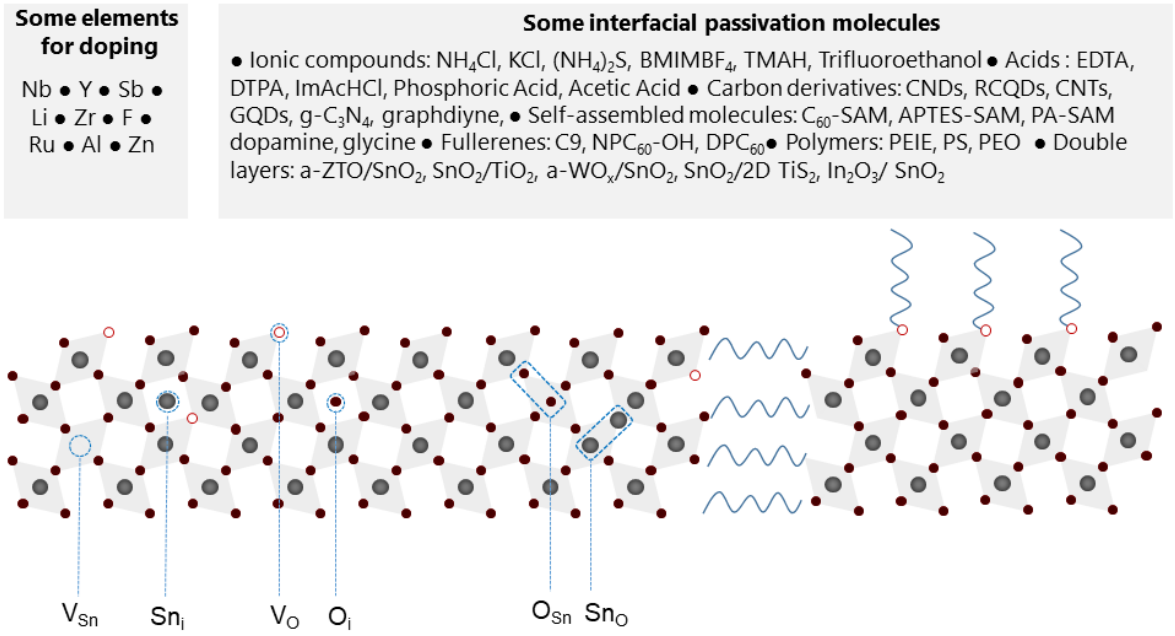

Figure 6. Sketch for the possible defects in rutile SnO_2 with potential passivation routes. Note: The full name of abbreviated compounds is given in the text.

5. Passivation routes for SnO_2 for high performance PSCs

5.1. Bulk passivation of SnO_2 by elemental doping

Doping of metal oxides with divalent metal cations (as listed in **Figure 6**) is an effective and proven method to enhance the electrical conductivity SnO_2, thereby reducing contact resistance and recombination at the ESL/perovskite interface, provided through a low CBM offset and the WF modification. As this results in enhanced PSC performance, this strategy has been extensively studied. The schematic of SnO_2 ESLs modification is given in **Figure 6**. For the pristine SnO_2 case, self-doping originating from the intrinsic defects dominates. However, the self-doping concentration of SnO_2 may vary greatly, depending on the processing conditions. Extrinsic ion doping can help improve the doping reliability and reproducibility. Ion doping can also improve the morphology of SnO_2 films prepared from a solution. In the case of extrinsic doping, several points need consideration: (i) the difference in valence between the dopant and host ions; for example, substituting Sn^{4+} with Sb^{5+} can significantly improve the conductivity of SnO_2, and (ii) the difference in atomic radius between the dopant and host ions

where the former is usually relatively smaller. (iii) the incorporation of extrinsic impurities may affect the carrier mobility through various scattering mechanisms and the formation of some possible secondary phases. Therefore, the doping processing parameters need to be adjusted to achieve optimal optoelectronic performance. So far, Al, Li, Nb, Ru, Sb, Y, Zn, Zr have been proven to be effective extrinsic dopants increasing the conductivity and mobility of SnO_2 films (see **Table 5**). Thanks to these improvements, the series resistances of the devices were decreased, which improved the *FF*, and reduced the hysteresis. Among these dopants, Ru, Y, and Nb have led to PCE values over 20%. So far, the choice of most of the reported elemental dopants was largely empirical, where their effectiveness was mainly judged via PCE values. However, this might not always be a reasonable strategy since the optimization of the other layers is also of importance. The above-mentioned criteria may guide readers to explore more efficient dopants.

Table 5. Some available bulk passivated SnO_2 ESLs and related parameters

Dopant		μ_e[a]	σ[b]	CBM[c].	N_t[d]	R_{rec}[e]	IR[f] [pm]	V_{oc} [V]	J_{sc} [mA cm^{-2}]	FF [%]	PCE [%]	Ref
Sb	Control						60	1.01	22.3	69.6	15.7	[34]
	Doped	n/a	↑	n/a	n/a	n/a		1.06	22.6	72	17.2	
Li	Control						76	1.084	21.98	64.17	15.29	[200]
	Doped	n/a	↑	↓	n/a	↓		1.106	23.27	70.71	18.20	
Al	Control						54	0.99[g]	21.72[g]	73.62[g]	15.80[g]	[201]
	Doped	↑	↑	↑	↓	n/a		1.06	22.78	75.41	18.2	
Zr/F	Control						72/133	1.089	23.06	69.1	17.35	[202]
	Doped	n/a	↑	↑	n/a	↓		1.105	24.39	71.2	19.19	
Zr	Control						72	1.06	24.8	66	17.30	[203]
	Doped	n/a	↑	↑	n/a	↓		1.08	25.3	72	19.54	
Zn	Control						74	1.11	22.72	75.1	18.95	[111]
	Doped	n/a	↑	↑	n/a	↓		1.12	23.41	77.3	20.16	
Nb	Control						72	1.144	21.43	75.20	19.69	[204]
	Doped	n/a	n/a	n/a	n/a	n/a		1.157	22.77	74.70	20.47	
Y	Control						90	1.074	22.44	75.04	18.08	[205]
	Doped	n/a	↑	↑	↓	n/a		1.13	23.56	77.78	20.71	
Ru	Control						56.5	1.10	24.10	76	20.2	[206]
	Doped	↑	↑	↑	↓	↓		1.15	24.60	78	22.0	

[a]Electron mobility; [b]conductivity; [c]conduction band minimum; [d]trap-state density; [e]recombination rate; [f]effective ionic radius[207]; [g]average PCE values. Note: ↑ and ↓ represents increase and decrease for related parameters after passivation.

5.2. Surface passivation of SnO_2

Ideally, passivation agents for the SnO_2/perovskite interface should simultaneously feature electro-negative and electro-positive functional groups to passivate under-coordinated tin

(electron-poor) and oxygen atoms (electron-rich). Upon the passivation, the surface dangling bonds associated with these under-coordinated surface atoms, and that act as recombination centers, are eliminated owing to the formation of new bonds between these specific surface atoms and the passivation agents. The resulting bonds can be covalent, ionic or Van der Waals in nature, depending on the molecular structure of the passivation molecule. Surface passivation can significantly influence the surface energy levels of SnO_2, and ideally, this should facilitate efficient charge extraction. Several strategies have been reported in the literature to mitigate the surface defects in the SnO_2 layer and can either take place during ESL synthesis or as a post-treatment. Moreover, interfacial layers underneath the perovskite may enhance the perovskite crystal quality and film coverage, which is beneficial to improve device performance and long-term stability.[78,208] Below, we discuss the most promising surface passivation techniques reported in the literature so far. The schematic illustrations of some of these techniques with different types of passivation molecules are sketched in **Figure 7** and **8**.

Ionic compounds

Ionic compounds accommodate electron-poor cations and electron-rich anions. Hence, they are highly efficient in regulating the under-coordinated oxygen and tin surface atoms, respectively. Positively charged cations can passivate surface V_{Sn}, O_{Sn}, and O_i defects, whereas negatively charged anions can passivate V_O, Sn_O, and Sn_i defects through electrostatic interaction. Notably, ionic compounds can simultaneously passivate the perovskite surface (including the grain boundaries) by diffusing into the perovskite layer. In this case, Zhu *et al.* reported that cations and anions respectively coordinate to halide and lead dangling bonds on the perovskite surface.[209]

Liu *et al.* added NH_4Cl into commercial col-SnO_2 (Alfa Aesar), which resulted in PSCs with the highest PCE (>21%) for samples with SnO_2 ESLs processed at 60 °C, at that time. Since NH_4^+ and Cl^- ions are smaller than MA^+ and I^- ions, the distance between the NH_4Cl layer and

SnO_2 becomes narrower, which improved the interface quality.[210] Later, Liang *et al.* followed the same strategy and achieved devices with a remarkable V_{OC} of 1.195 V.[211] Alkaline chloride salts are also efficient passivating compounds for the interfaces between metal oxides (*e.g.*, TiO_2[66], NiO_x[212], and SnO_2[209]) and perovskites. In 2017, Tan *et al.* attached Cl ligands to TiO_2 NCs, resulting in a stronger binding between TiO_2 and perovskite, and one of the highest PCE values for compact devices at that time (see **Infographic 1** and **Table 1**).[66] In 2019, Zhu *et al.*, applied the same strategy to SnO_2 NCs (Alfa Aesar), this time by using KCl as an additive to obtain the additional passivation effect from K^+ at perovskite grain boundaries, and achieved PCEs up to of 22.2% (21.6% stabilized).[209,213]

In a comparative study, Liu *et al.* studied the effect of PCBM, choline chloride, KI, and KCl as SnO_2 surface passivation agents. They found that all tested molecules improved the device performances remarkably except from PCBM.[214] The main reason is that such molecules feature both anion and cations ($choline^+$, K^+, I^-, Cl^-), which can passivate simultaneously positively and negatively charged ionic defects at the perovskite/SnO_2 interface. However, among these materials, only KCl passivated devices could remove the hysteresis, resulting in a champion PCE of 20.5% (stabilized 20.5%) with long-term stability (90% of its initial efficiency after 30 days). In a similar way, tetramethylammonium hydroxide (TMAH, $N(CH_3)_4OH$) ionic liquid was used as an additive to SnO_2 NCs colloidal dispersions, resulting in an improved conductivity.[215] Similarly, Noel *et al.* treated the SnO_2 layer with 1-butyl-3-methylimidazolium tetrafluoroborate ($BMIMBF_4$), and found that this decreases the work function of SnO_2 but also shifts the perovskite Fermi level towards the CBM, resulting in a more *n*-type character of the perovskite.[216] Overall, among all these reported ionic liquids, KCl and NH_4Cl seem more effective than others due to their simultaneous passivation of positively and negatively charged defects.

Carbon Derivatives

Carbon derivatives find wide applications in PSCs thanks to their various functionalities.[217] To passivate the SnO_2 surface, carbon nano-dots (CNDs)[218] and quantum dots (CQDs)[219] were utilized due to their carboxylic-acid- and hydroxyl-rich surfaces, and carbon nanotubes[220] due to their high conductivity. The results for the carbon-based passivation compounds are summarized in **Table 6**. Notably, PSCs with red-CQD passivated SnO_2 as ESL reached among the highest PCE values in literature (22.77%) with shelf stability up to 1000 h (dark conditions, 40% RH).[219] In the future, SnO_2 based PSCs may further exploit benefits from carbon derivatives as a dopant, capping layer, or a passivation compounds resulting in enhanced operational stability.

Acids

Compounds with carboxylic- and phosphonic-acid functional groups are commonly used to passivate metal oxide surfaces. For carboxylic acid functional groups, several binding modes, such as electrostatic attraction, H-bond to bridging oxygen, H-bonds to carboxylic oxygen, monodentate (metal–ester), bidentate bridging or bidentate chelating, are possible.[221,222] For instance, acetic acid is a good option as one of the simplest carboxylic acids with a methyl group attached to a carboxyl group.[223] Ethylenediaminetetraacetic acid (EDTA), is another successful example with a strong chelation function which provides strong interaction with metal atoms.[224] Moreover, their hydrophilic nature promotes the growth and grain size of perovskite. Diethylenetriaminepentaacetic acid (DTPA, or pentetic acid) is another industry-relevant chelating agent that is structurally very similar to EDTA, also helped to achieve 1000 h under ambient conditions by preserving 98% of its initial PCE (~21.28%).[70] 4-imidazoleacetic acid hydrochloride (ImAcHCl) is also known as an ionic compound which can provide a chemical bridge between perovskite and SnO_2 (**Figure 8**).[225] Phosphoric acids [R-PO_3H_2] and phosphonate ester derivatives [R-PO_3R_2] (where R = alkyl or aryl) are amongst the most commonly used compounds as they can easily react with oxide surfaces by forming

phosphonate bonds. For example, phosphoric acid can terminate Sn dangling bonds on the surface of the SnO_2 films by forming Sn–O–P bonds.[226] This reduces the potential barrier induced by O^{2-} ions which is formed due to the electron capturing of O^- from the CB of SnO_2. Among the reported acids, EDTA made the most notable change compared the control devices by increasing the PCE values with an absolute value of 2.59% and prolonging the shelf stability to 2880 h without encapsulation. Overall, acid treatments appear to be attractive options for scaled PSC manufacturing, especially when using industry-relevant chemicals with self-limiting reactions with metals. However, ultimately, additional functionalization may be required resulting in e.g. the simultaneous passivation of positive and negative defects at both the SnO_2 and perovskite sides.

Self-assembled molecules (SAMs)

Interface modification with SAMs usually aim to adjust the WF and surface energy of metal oxides by forming a permanent dipole moment resulting from the ordered molecular alignment at the interface. In addition, they passivate inorganic surface states by making diverse chemical interactions between the ESLs and ionic perovskites, and thus tune the interfacial optoelectronic properties.[227-230] SAMs generally consist of three key groups; an anchoring group, a linker, and a functional group. The functional group determines surface properties and interacts with the perovskite. The linker group provides a well-defined thickness and may act as a physical barrier. The anchoring group covalently binds to metal oxide surfaces via different attachment chemistries such as phosphonates, carboxylates, silanes, catechols, alkynes and alkenes, and amines. Each of these attachment chemistries has different binding strengths with metal oxide surfaces, depending on the reactivity of the anchoring group, the nature of the oxide surface, and reaction conditions. The anchoring mechanism and binding mode (monodentate, bidentate, tridentate) greatly depends on Lewis acidity of metal oxide surface. Nonetheless, all reaction pathways proceed through either covalent bond formation between electron-rich SAM atoms

and Lewis acid sites (oxygen-deficient) on metal oxides or electron-poor SAM atoms and Lewis base sites (oxygen saturated) on metal oxides. SAMs with carboxylic acid functional groups can react with both tin and oxygen dangling bonds on the SnO_2 surface, and thus, passivate the surface with high coverage. As an example, the C_{60} self-assembled monolayer (C_{60}-SAM) can be used for effective passivation of SnO_2, where the C_{60} functional group facilitates electron transfer from the perovskite layer to the SnO_2 ESL due to its high electron affinity (**Figure 7**).[186,231,232] Similarly, applying C_{60}-Catechol-, C_{60}-Phenylphosphoric acid, PCBM-Benzoic acid-SAMs to SnO_2 ESLs may find future applications to realize highly efficient PSCs. SAMs incorporating alkoxysilane or hydroxysilane anchoring groups such as 3-aminopropyltriethoxysilane (APTES)-SAM have also been studied, as they readily react with –OH groups on SnO_2 (**Figure 7**).[230] Furthermore, these molecules can provide more intimate contact between SnO_2 and the perovskite, resulting from the surface wetting property of APTES-SAM, as well as perovskite morphology improvement.[230] The schematic illustration of modifying the SnO_2/perovskite interface with the SAM molecules studied to date is shown in **Figure 7** (see also **Table 6** for related device performances). Overall, a rich library of SAM molecules, combined with a high process reproducibility, makes this a promising option for scalable PSCs.

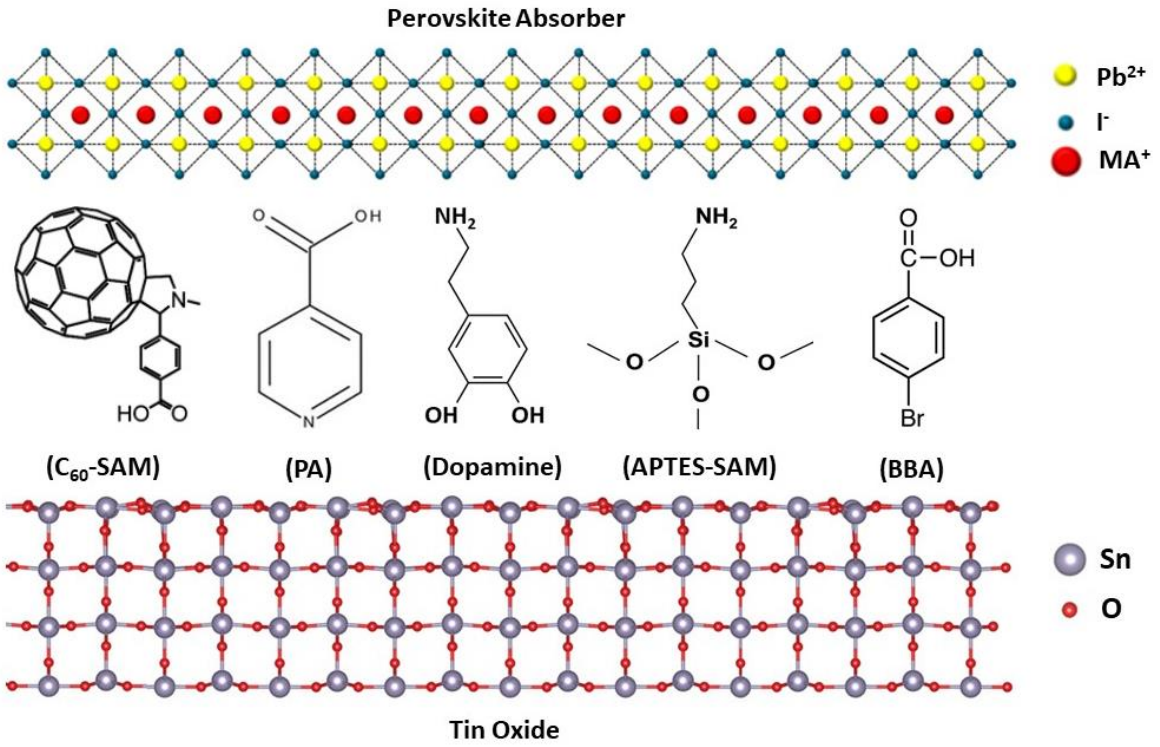

Figure 7. Illustration of tuning the SnO_2 ESL/perovskite interface with various SAMs. (PA, 4-pyridinecarboxylic acid; BBA, 4-Bromobenzoic acid) Reproduced with permission.[227,233] Copyright 2016, American Chemical Society; Copyright 2019, Wiley-VCH.

Fullerene derivatives

Similar to the C_{60}-SAM, several fullerene derivatives can self-assemble on the SnO_2 surface and facilitate electron extraction from the perovskite layer. Here, we discuss these separately because it is usually not reported whether these fullerene derivatives form a monolayer or multi-layer on the SnO_2 surface. As an example, C9 (9-(1-(6-(3,5-bis(hydroxymethyl)phenoxy)-1-hexyl)-1H-1,2,3-triazol-4-yl)-1-nonyl[60] fullerenoacetate) is a promising passivant for SnO_2 since it shows a strong electron affinity and well-matched lowest unoccupied molecular orbital (LUMO) level with the perovskite band structure (**Figure 8**). Also, its -OH terminal groups can passivate O_v on the surface of SnO_2.[234] Another fullerene derivative is pyrolidinofullerene C_{60}-substituted phenol (NPC_{60}-OH), which was proposed since it forms interfacial dipoles at the SnO_2/perovskite interface, which stems from the functional phenolic hydroxyl group of NPC_{60}-OH. This leads to a decreased WF of SnO_2 and thus reduced the CB offset at the

SnO_2/perovskite interface, and also helped to increase of perovskite grain size due to the hydrophobicity nature of the molecule.[235] Finally, the *cis*-fullerene derivative of 2,5-diphenyl C_{60} fulleropyrrolidine (DPC_{60}) offers simultaneous passivation of the perovskite and SnO_2 sides, where the *cis*-configuration of the phenyl groups improves the interface quality between DPC_{60} and perovskite due to its small steric hindrance (**Figure 8**).[236]

Polymers

Polymers are frequently used to modify the SnO_2 surface since they can attach to these surfaces with many monomeric units. The cumulative Van der Waals interaction may provide a sufficiently strong binding between the polymers and the SnO_2. Ethoxylated polyethyleneimine (PEIE) is a particularly well-studied polyelectrolyte which contains simple aliphatic amine groups and can tune the WF of the metal oxides due to the induced interfacial dipoles.[237-239] It is also found to be an effective passivation material for SnO_2 and enables an improved perovskite crystal quality.[240,241] Polystyrene (PS) is another widely used polymer for the passivation of PSCs, which was also applied to the SnO_2/perovskite interface.[242] At the interface, PS reduces the thermal expansion mismatch between perovskite and SnO_2 due to its low glass transition temperature (T_g, 65 °C), which as a result decreases the film stress during the perovskite film formation. In addition, PS can passivate the SnO_2/perovskite interface defects as well as the perovskite top surface, simultaneously shielding the perovskite from humidity. Next, polyethylene oxide (PEO, also known as polyethylene glycol) was used to form a crosslinking complex between the perovskite and metal ions in SnO_2, providing thereby bulk passivation of the perovskite and surface passivation of the SnO_2 film.[241,243] Moreover, PEG incorporation enhances the surface wettability of SnO_2, which benefits the deposition of uniform and pinhole-free perovskites onto SnO_2. Overall, although many successful polymers have been reported with enhanced V_{OC}, the insulating nature of the polymers mostly causes *FF* losses due to the increased contact resistivity. Therefore, the thickness of the layers (based on

the surface roughness of the SnO_2 layers) should be controlled carefully to avoid the increased contact resistivity. Compared to the SAM approach, polymer passivation may also suffer from reproducibility issues.

Other Compounds

Alternatively, triphenylphosphine oxide (TPPO) is used as an inexpensive and air-stable electron donor to passivate the SnO_2 surface due to the strong interaction of TPPO with SnO_2, induced by surface delocalized electrons.[233] This increases the electrical conductivity and decreases the energy barrier at the SnO_2/perovskite interface. As being in TPPO case, more compounds can be used in SnO_2 based PSCs to improve the performance in the future. The impact of various passivation molecules on the Voc of devices using SnO_2 ESLs is demonstrated in **Figure 9**.

Table 6. Summary of surface passivation strategies for low-temperature processed SnO_2 ESLs.

Passivator	PFG[a]	CBM[b]	N_t[c]	R_{rec}[d]		V_{oc} [V]	J_{sc} [mA cm^{-2}]	FF [%]	PCE [%]	Ref
Ionic compounds										
$BMIMBF_4$	$BMIM^+$, BF_4^-	↑	↓	↓	Control	1.13	22.4	75	19.2	[197]
					Passivated	1.16	22.7	79	20.8	
NH_4Cl	$-NH_4^+$, $-Cl^-$	↓	↓	↓	Control	1.10	23.22	73.47	18.71	[210]
					Passivated	1.15	24.28	76.83	21.38	
KCl	K^+, Cl^-	↓	↓	↓	Control	1.077	24	77.9	20.2	[209]
					Passivated	1.137	24.2	80.7	22.2	
$(NH_4)_2S$	S^{-2}	↑		↓	Control	1.13	22.40	73.41	18.67	[244]
					Passivated	1.15	22.95	75.95	20.03	
TMAH	$-N(CH_3)_4^+$, -OH	↑			Control	1.13	22.80	70.43	18.14	[215]
					Passivated	1.14	22.51	79	20.28	
Trifluoroethanol	F^-, O donor	↑	↓	↓	Control	1.10	23.12	78	19.17	[245]
					Passivated	1.12	23.91	75.5	20.92	
Acids										
EDTA	-COOH	↑	↓	↓	Control	1.10	22.79	75.5	18.93	[224]
					Passivated	1.11	24.57	79.2	21.60	
DTPA	-COOH			↓	Control	1.06	24.71	77.01	20.09	[70]
					Passivated	1.12	24.68	76.73	21.18	
ImAcHCl	-COOH, Ester bond	↑	↓	↓	Control	1.089	22.65	79	19.53	[225]
					Passivated	1.153	23.06	79	20.96	
Acetic Acid (CH_3CO_2H)	Ac	↑	↓	↓	Control	1.141	22.07	74.8	18.84	[223]
					Passivated	1.158	22.39	79.3	20.56	
Phosphoric Acid (H_3PO_4)	P, -OH	↓		↓	Control	1.18	22.54	73.81	19.67	[226]
					Passivated	1.17	23.20	77.40	21.02	
Carbon Derivatives										
CNDs	CNDs	↓	↓	↓	Control	1.08	22.51	76	18.54	[218]
					Passivated	1.10	23.14	79	20.03	
RCQDs	RCQDs		↓	↓	Control	1.07	23.1	77.8	19.15	[219]
					Passivated	1.14	23.3	82.9	22.77	
CNTs	CNTs	↓	↓	↓	Control	1.09	22.32	73.90	17.90	[220]
					Passivated	1.12	23.26	78.23	20.33	
GQDs	GQDs	↑	↓	↑	Control	1.101	22.10	73.6	17.91	[246]
					Passivated	1.134	23.05	77.8	20.31	
$g\text{-}C_3N_4$	$g\text{-}C_3N_4$	↑	↓	↓	Control	1.118	23.72	76.2	20.21	[247]

					Passivated	1.176	24.03	78.3	22.13	
Self-assembled Monolayers										
C_{60}	-COOH				Control	1.09	21.74	73.23	17.34	[186]
					Passivated	1.12	21.78	77.87	18.95	
PA[e]	-COOH				Control	1.06	21.65	74.9	17.19	[227]
		↑	↑		Passivated	1.10	22.03	77.4	18.77	
Dopamine	-NH_3, OH				Control	1.04	19.96	67.6	14.05	[228]
		↑	↓	↓	Passivated	1.05	21.80	73.9	16.87	
APTES	-NH_2, OH				Control	1.065	20.84	66.2	14.69	[230]
		↓			Passivated	1.16	21.23	69.2	17.03	
Glycine[f]	NH_2, COOH	↑		↓	Control	1.06	22.50	78.10	18.82	[248]
					Passivated	1.10	24.16	77.08	20.63	
Fullerene Derivatives										
C9	-OH	↑	↓	↓	Control	1.10	23.2	78.2	20	[234]
					Passivated	1.12	24.1	78.9	21.3	
NPC_{60}-OH	-OH	↑	↓	↓	Control	1.11	22.67	75.86	19.04	[235]
					Passivated	1.13	23.37	80.73	21.39	
DPC_{60}	N-H	↑			Control	1.11	22.5	75.5	18.8	[236]
					Passivated	1.14	23	77.7	20.4	
Polymers										
PS	Aromatic ring		↓	↓	Control	1.085	23.8	74	19.3	[242]
					Passivated	1.097	23.95	76	20.5	
PEIE	Aromatic ring, -NH_2, I^-	↑		↓	Control	1.08/	22.92	76	18.74	[240]
					Passivated	1.14	23.83	76	20.61	
PEO	-C=O, -COOH				Control	1.09	22.62	77.9	19.2	[241]
					Passivated	1.12	22.67	81.9	20.8	
Other Compounds										
TPPO	O donor	↑		↓	Control	1.079	24.40/	72.22	19.01	[233]
					Passivated	1.106	24.30	76.40	20.69	

[a)]passivation functional group; [b)]conduction band minimum, [c)]trap-state density, [d)]recombination rate; [e)]4-pyridinecarboxylic acid; [f)]$C_2H_5NO_2$.

↑ and ↓ denote the increase and decrease for related parameters after passivation of SnO_2 ESLs, respectively.

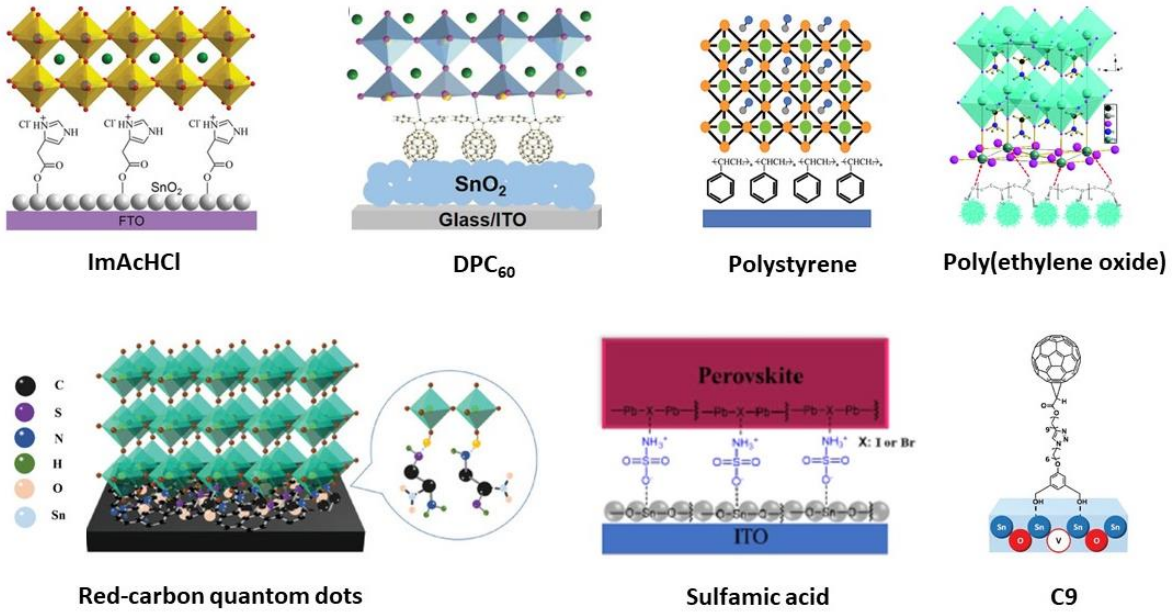

Figure 8. Schematic drawing of various functional molecules between SnO_2 ESL and perovskite. Note: DPC_{60}: 2,5-diphenyl C_{60} fulleropyrrolidine; ImAcHCl: 4-imidazoleaceticacid hydrochloride. Reproduced with permission.[219,225,234,236,242,243,249] Copyright 2018, The Royal Society of Chemistry; Copyright 2019, Wiley-VCH; Copyright 2020, American Chemical Society.

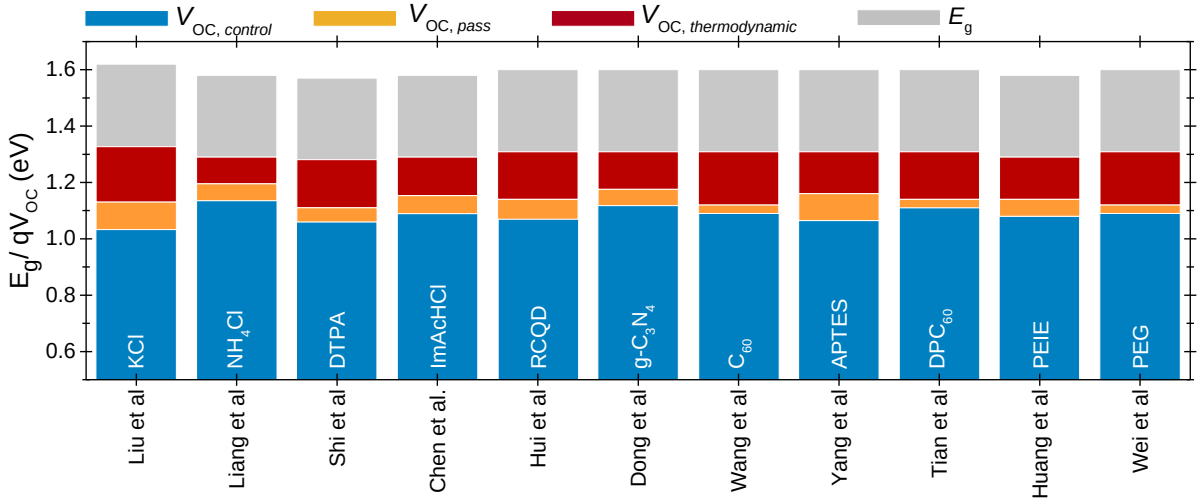

Figure 9. The influence of the various passivation routes on SnO_2 electrodes on the V_{OC} of the PSCs. The reported values are taken from **Table 6**. $V_{OC,\ thermodynamic}$ values taken from the detailed balance limit parameters for a single-junction solar cell as a function of E_g.[250]

5.3. Double layer configuration of SnO_2 with other metal oxide layers

Combining different inorganic ESLs may offer a pinhole-free, smooth and compact architecture, benefiting from the individual advantages of the involved materials.[251] Also, a double-layer ESL may enable a graded band alignment, which can enhance carrier extraction, the V_{OC}, and the overall surface morphology.[252] These double-layer ESLs can either be in homojunction form such as Sb-doped SnO_2/SnO_2,[253] or in heterojunction form such as SnO_2/TiO_2,[254] SnO_2/2D TiS_2,[255] amorphous-WO_x/SnO_2,[256] or amorphous-Zn_2SnO_4/SnO_2.[257] Overall, such stacks target the improvement of at least one parameter of SnO_2 contacts as shown in **Table 7**. For example, SnO_2/TiO_2 contacts can provide gradient band alignment,[254] whereas, SnO_2/2D TiS_2 (with ultrathin 5 nm, TiS_2) can establish a better interface with a strong chemical affinity of Pb for SO_4^{2-} groups and passivates the trap states.[255] Alternatively, an interlayer can be positioned at the TCO/SnO_2 interface to decrease the roughness of SnO_2, resulting in pinhole-free perovskite film.[258] Additionally, hybrid deposition methods (for example, SnO_2 by solution processing, second layer by ALD) can also be utilized to exploit specific advantages of the involved techniques, as discussed in **Section 3** in detail. With double layer ESLs, one of the highest certified PCEs in literature (22.54%) was

achieved by inserting In_2O_3 between the ITO electrode and SnO_2.[258] Nevertheless, while choosing the interlayer, possible associated detrimental effects need to be considered carefully, since SnO_2 is already superior to many inorganic materials (see **Table 1**). For example, PSCs using bilayer SnO_2/TiO_2 ESLs exhibit a reduced stability against UV illumination due to the photocatalysis effect of TiO_2.[251,259] Overall, for scalability perspective, double-layer configurations may be less promising compared to other methods, due to the requirement of additional processing.

Table 7. Survey of double-layer configurations for PSCs using low-temperature processed SnO_2

ESL Structure		CBM[a] of ESL [eV]	CBM of Perovskite [eV]	PCE[b] [%]	HI[d] [%]	Remaining Performance of its initial PCE After Stability test [%]	Stability Condition	Ref
a-ZTO	Control	-4.38	-3.92	17.10		N/A	210 h, ambient cond.	[257]
a-ZTO/SnO_2*	Target	-4.25		20.04	↓	90%		
SnO_2	Control	4.33	-3.60	18.09	3.34	100	49 days, N_2, RT	[254]
SnO_2/TiO_2*	Target	-4.10		20.50	6.05	100		
SnO_2	Control	-4.41	-3.9	17.67		N/A	35 days, N_2 and 40% RH	[256]
a-WO_x*/SnO_2	Target	-4.24		20.52	↓	95%, 85%		
Sb:SnO_2	Control	-4.54	4.20	19.15	6	73	2280 h, 50% RH, RT	[253]
Sb:SnO_2/SnO_2*	Target	-4.43		20.73	2.46	80		
c-TiO_2 (450 °C)	Control	-4.3	-4.22	17.03		<40	200 h, 35% RH, 80 °C	[251]
c-TiO_2/SnO_2*	Target	-4.24		20.98	↓	>95		
SnO_2 NPs	Control	-4.06	4.20	17.92		59	1200 h, 25% RH	[260]
SnO_2 NPs/$SnCl_2.2H_2O$*	Target	-4.31		21.09	↓	83	1400 h, 25% RH, RT	
SnO_2	Control	-4.68	-4.36	19.65		87.2	800 h, 10% RH, RT	[255]
SnO_2/2D TiS_2*	Target	-4.63		21.73	↓	92		
SnO_2	Control	-4.2	-3.85	21.42		92.7	80 days, N_2, RT	[258]
In_2O_3*/ SnO_2	Target	-4.55		23.24	↓	97.5		

[a]conduction band minimum; [b]all efficiency results are acquired reverse-scan bias direction; [c]hysteresis index, HI:$\Delta PCE = |(PCE_{reverse} - PCE_{forward})|$; * indicates conduction band energy for related layer in the next column.

6. SnO_2 contacts in flexible perovskite solar cells

Flexible solar cells may offer a high power-per-weight ratio and comparably low manufacture cost (due to band-to-band and roll-to-roll fabrication feasibility) with comparison to their rigid counterparts. The inherent mechanical flexibility of metal halide perovskites enables compatibility with roll-to-roll production of flexible PSCs (flex-PSCs), which is attractive for large-scale production. As the required annealing temperature for perovskites is mostly in the range of 70 to 150 °C, their fabrication can be made compatible with common flexible foils as substrates such as polyethylene terephthalate (PET, T_g: 70-110 °C)[96] and polyethylene

naphthalate (PEN, T_g: 120-155 °C),[96] without resulting in severe deformation.[261,262] To achieve successful flex-PSCs, transparent electrodes and charge selective layers, along with the perovskite absorbers, should satisfy similar requirements. Here, we focus only on SnO_2 ESLs on flexible substrates. We encourage the readers to also read at the reviews by Jung *et al.*,[96] Zang *et al.*,[139] and Di Giacomo *et al*.[263] to learn more about requirements for the other layers in flexible solar cells.

Following TCO deposition, the first step to fabricate the flexible solar cells is adapting the charge selective layer processes for flexible substrates since they pose inferior surface morphology (high roughness) and lower transmittance compared to the rigid ones such as glass.[36] Such meticulous tailoring of the ESL on flexible substrates is needed to minimize the efficiency offset between flexible and rigid devices. For example, the surface roughness of the ITO/PEN foils (2.79 nm) is higher than ITO/glass (1.69 nm).[36] Although the difference in roughness seems marginal, carefully controlling the thickness of the films enabled a 19.51% PCE (20.41% for the same recipe on glass) on PET substrates. Also, these devices maintained 95% of their initial PCE after 6000 bending cycles, and 90% after more than 1000 h shelf stability (RH 10%), demonstrating the outstanding capability of flex-PSCs.

Another common problem with the solution-processed SnO_2 is the removal of the surfactants at low temperatures, which usually exist in col-SnO_2 solutions to maintain the dispersion. If this surfactant is not removed, it leads to a high resistivity of the as-deposited SnO_2 films. To address this issue, we explained the usage of room-temperature plasma treatments in **Section 3.2**. In flex-PSCs, the same strategy can lower the processing temperature of SnO_2 as low as 80 °C.[92,264] The effectiveness of UV-ozone treatments was also verified over a large area with PCE of 12.50% and a V_{OC} of 6.496 V for a 5 × 5 cm^2 flexible mini-module (six series-connected cells), while small area devices gave PCEs of 16.50% with almost no hysteresis.[102] Alternatively, hydrothermal treatments (at 100 °C) can also be utilized to take advantage of the

high vapor pressure of water, which helps to enhance connectivity between grain boundaries and leads to denser SnO_2 NPs by grain squeezing.[262] This method resulted in champion and certified PCEs of 18.1% and 17.3%, respectively (the highest reported certified PCE for flex-PSCs as of 2020, August). These cells also achieved good mechanical stability by maintaining 80% of their initial PCE even after being bent 1000 times with 14 mm bending curvature. Using additives may eliminate the need for either annealing above 100 °C or UV-ozone treatments, and this leads to highly uniform and dense surfaces. For example, tert-butanol (TBA) as an additive into a col-SnO_2 solution (Alfa Aesar) helps to obtain highly uniform films on ITO/PEN substrates, where methyl group on TBA increases the surface wettability and helps to achieve denser films.[265] Another method to obtain denser films is to reduce the size of NCs. For this, specialized synthesis techniques such as reverse micelle water injection can lead to SnO_2 QDs with an average size as small as 2.9 nm[110], compared to ≈ 4-5 nm for Alfa Aesar col-SnO_2 NCs.[136] Flex-PSCs based on such SnO_2 ESLs achieved a PCE of 17.7% with notable mechanical stability by retaining 92% of its initial efficiency after 1000 times bending trial (18 mm bending radius), which is a good indicator for commercial applicability.

For scalable devices, high-throughput techniques (which are discussed in **Section 3**) such as slot-die coating of col-SnO_2 seems particularly promising with its suitability to roll-to-roll processing and ease of access to raw materials. With this technique, a PCE of 15.22% (active area of 16.07 cm^2, **Figure 10**) was achieved with negligible hysteresis and long term stability, preserving 80% of its initial PCE after 1000h shelf stability (RH of 20%) without encapsulation.[41] Also, the mechanical stability of related modules was remarkably high, with no more than 30% PCE decay even after 1800 bending cycles. In the roll-to-roll approach, gravure-printing is another proven method, where the printing cylinder is partially immersed in the col-SnO_2 container, filling the engravings. This pattern is then transferred from the cylinder to a substrate to form SnO_2 ESLs on flexible substrates.[42] To have a continuous process, hot

air blowing (120 °C) was applied to remove the surfactants, which resulted in a champion (average) PCE of 17.2% (16.0%).

Vacuum based techniques are attractive to process amorphous films; the amorphous nature can aid the mechanical durability of SnO_2 films. As discussed in **Section 3.2** in detail, ALD is a scalable technique to achieve highly-efficient PSCs. However, fabricating high-quality SnO_2 layers with temperatures <100 °C by thermal ALD is challenging since the resultant films contain impurities,[266] which can result in a relatively high film resistivity. Plasma-enhanced ALD (PE-ALD) technique can be used to solve this issue.[267] This technique allows the surface to be exposed to plasma-generated species during the thermal surface reactions, and consequently, enables a better film quality at lower temperatures. However, PE-ALD grown SnO_2 films remained amorphous with poor electrical conductivity and low electron mobility, preventing further improvement in device performance. To overcome this issue, a post-annealing treatment at 100 °C in the presence of water vapor can be used to alleviate the complete reaction of organic materials, resulting in purer SnO_2films.[267] Following these steps and utilizing C_{60}-SAM passivation, a PCE of 18.36% (stabilized 17.02%) was achieved. Although the reported devices here were <0.1 cm^2, this technique carries a high potential for large scale deployment of SnO_2 contacts high efficiency devices. Note that, the aforementioned passivation strategies in **Section 5** can also be applied to flex-PSCs. For example, KCl modification on SnO_2 (spin casted col-SnO_2) leads a FF of 81% with a PCE of 18.53%, which underlines the universality of the discussed techniques in this review.[268]

Overall, there are several ways to process SnO_2 films on temperature-sensitive substrates with scalable methods. We summarized the SnO_2 ESLs based flex-PSCs having PCE over 15% reported in the literature in **Table 8**, from which one can find that fabrication techniques and annealing temperatures of SnO_2 ESLs, together with structures of related devices and their active areas used during J-V measurement. Also, **Figure 10** shows several images of reported

small area PSCs and mini-modules, as well as effect of mechanical bending on flexible devices using SnO_2 ESLs. On the other hand, to achieve high performance PSCs, the processing temperature of the other layers, including perovskite absorber, should also be engineered carefully. For flexible substrates, NC-based SnO_2 films work well thanks to the high elastic stiffness of nanocrystal assemblies.[269,270] For further designs, the actual operational conditions (heating-cooling cycles) and coefficient of thermal expansion values of the layers, as well as the bending durability (**Figure 10c, d** and **e**) should be considered to find ways to mitigate mechanical stresses. For this, industrial testing protocols should increasingly be considered.[271]

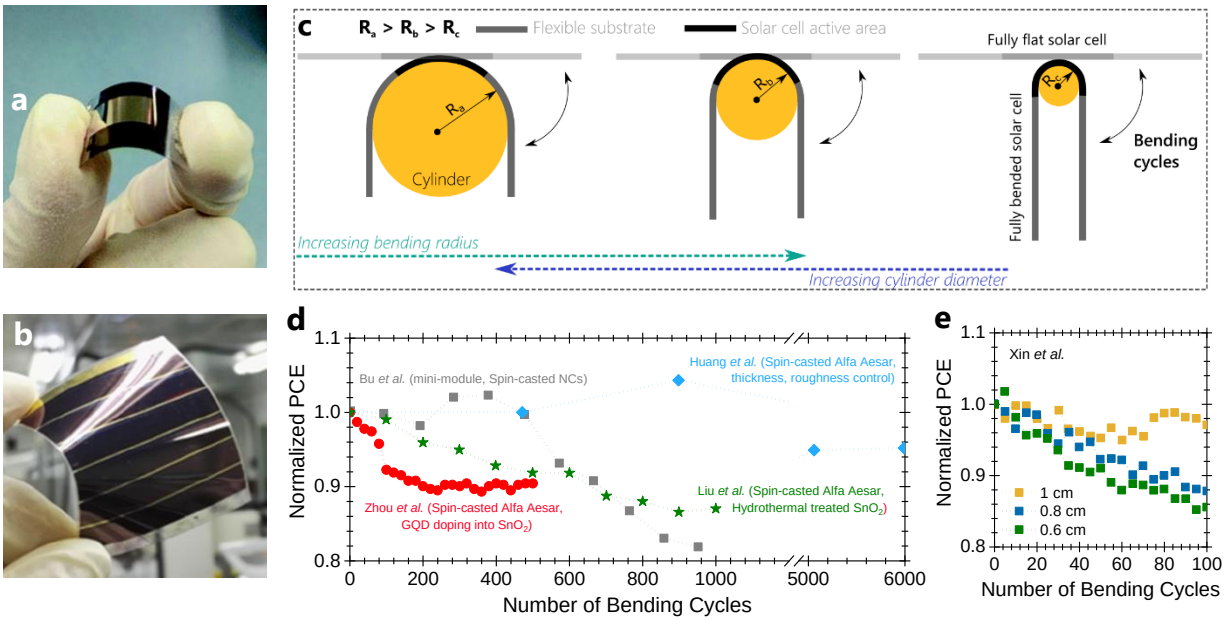

Figure 10. The photograph of the a) single cell and b) mini-module flex-PSCs. c) The sketch for the bending tests of flex-PSCs, which demonstrates the effect of the bending radius. d) The PCE evolution of flex-PSCs with an increasing number of bending cycles. e) Influence of the bending radius on the PCE of the devices. a) Reproduced with permission.[264] Copyright 2019, The Royal Society of Chemistry. b) Reproduced with permission.[41] Copyright 2018, Springer Nature. d) Panel d is produced from different studies reported in **Table 8**. e) Panel e is replotted from ref.[265]

Table 8: The fabrication methods of SnO_2 ESLs for flex-PSCs. The precursor, annealing temperature, device configuration, active area, and PCE parameters are also indicated.

Method	Precursor	T [°C]	Device Structure	Area [cm^2]	PCE [%]	Ref
SC[a]	Col-SnO_2	100	PET/ITO/SnO_2/KCl/Perovskite /Spiro/Ag	0.04	18.53	[268]
R2R[b]	Col-SnO_2	120	PET/ITO/ SnO_2/Perovskite /Spiro/Ag	0.052	17.2	[42]
PEALD[c]	TDMASn	100	PET/ITO/ SnO_2/C_{60}-SAM/Perovskite /Spiro/Au	0.08	18.36	[267]
SC	SnO_2 NPs	150	PEN/ITO/ SnO_2/Perovskite /Spiro/Au	0.09	15.07	[215]
SC	Col-SnO_2	150	PEN/ITO/ SnO_2/Perovskite /Spiro/Ag	0.09	19.51	[36]
SC-HT[d]	Col-SnO_2	100	PEN/ITO/ SnO_2/C_{60}/Perovskite /Spiro/Au	0.1	18.10	[262]
SC-NPT[e]	$SnCl_4.5H_2O$	RT[f]	PET/ITO/ SnO_2/Al_2O_3/Perovskite /Spiro/Au	0.12	18.1	[134]
SC	Col-SnO_2	60	PET/ITO/ SnO_2/Perovskite /Spiro/Au	0.12	18.28	[224]
SC	SnO_2 QDs	100	PEN/ITO/ SnO_2/Perovskite /Spiro/Au	0.14	17.7	[110]
SC	SnO_2 NCs	50	PEN/ITO/ SnO_2/Perovskite /Spiro/Au	0.16	16.11	[92]
SC	SnO_2 NCs	130	PEN/ITO/ SnO_2/Perovskite /Spiro/Ag	N/A	18.00	[183]
SC	SnO_2 NCs	120	PET/ITO/ SnO_2/Perovskite /Spiro/Au	10	12.40	[102]

[a]Spin-coating; [b]Roll-to-roll printing; [c]Plasma-enhanced ALD; [d]Hydrothermal; [e]N_2 Plasma Treatment; [f] Room Temperature. All efficiencies are taken from reverse-scan bias direction.

7. SnO_2 buffer layers in perovskite-based tandem solar cells

For the successful market entrance of PSCs, integration with established solar cell technologies (*e.g.*, c-Si, CIGS) may be an attractive path.[272] In tandem solar cells, two different absorber materials are stacked to harvest more efficiently the incident solar spectrum, resulting in higher PCE values. Here, thanks to their bandgap that can be tuned to fairly large values, PSCs are usually employed as top cells (sunward side) of such tandem devices, which absorbs the blue portion of the spectrum and transmits the rest of the solar spectrum to the narrow bandgap bottom sub-cell.

Experimentally, fabricating perovskite top cells is more complicated than single-junction (opaque) devices since they require highly transparent electrodes at their front such as ITO, indium-doped ZnO (IZO), zirconium-doped In_2O_3 (IZRO), and H: In_2O_3 for charge collection.[273-276] Here, the widely used sputtering technique may lead to degradation of the underlying soft layers due to impingement of highly energetic particles and plasma luminescence generated during deposition. Therefore, utilizing buffer layers is inevitable for protection. Initially, nanoparticles such as ZnO and aluminum-doped ZnO (AZO) were tested for this purpose.[273] Later, ALD processed buffer layers were found to be more promising due to their amorphous nature (resulting in a high coverage) and high conformity.

Here, SnO_2 stands out as the most promising among metal oxide buffers (*e.g.*, ZnO, TiO_2) due to its high conductivity (as discussed in detail in **Section 2**) and its dual function, serving simultaneously as efficient ESL and buffer layer. Today, most of the state-of-the-art tandem solar cells employ ALD SnO_2 buffer layers. **Figure** 11 shows three major concepts of perovskite/silicon tandem solar cells, each with their own specific perovskite top surface roughness. It was found that ALD SnO_2 functions as an efficient buffer layer even on pyramidal textured silicon wafers (pyramid size of several microns). Additionally, efficient perovskite/CIGS tandems also incorporate SnO_2 layers acting both as recombination and buffer layer. In perovskite/perovskite tandems, ALD SnO_2 acts as a good chemical barrier which helps to prevent the dissolution underlying perovskite layer by polar aprotic solvents.[273]

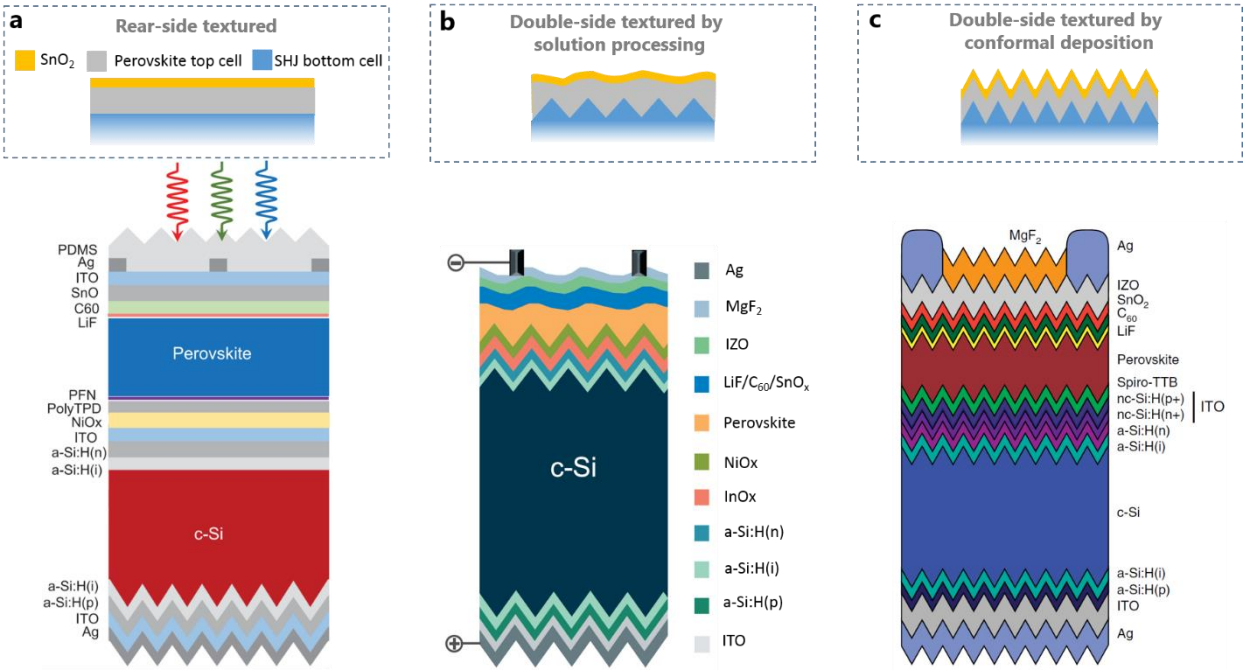

Figure 11. The sketch illustration the utilization of ALD SnO_2 buffer layers in perovskite/silicon tandem solar cell with different surface texturing of a) rear side textured, b) double-side textured by solution processing and, c) double-side textured by conformal deposition. a) Reproduced with permission.[277] Copyright 2020, The American Association for the Advancement of Science. b) Reproduced with permission.[3] Copyright 2020, The American Association for the Advancement of Science. c) Reproduced with permission.[278] Copyright 2018, Springer Nature.

8. Techno-economic analysis of SnO_2

Considering the success of SnO_2 in PSCs, the sustainability of this material for large-scale production is a natural question that arises quickly. Relatedly, this section discusses the economic feasibility and sustainability of this material. In nature, Sn(IV) oxide can be found in the form of cassiterite[195], which requires a high-cost purification process. Metallic Sn is extracted from the cassiterite and used to produce a highly pure SnO_2 based on simple oxidation process in air.[279] This process enables an annual production of SnO_2 of several hundreds of kilotons (we predicted according to tin mining production of 300.000 tons per year).[195] As well as being efficient contacts in solar cells, SnO_2 is an important material for different industrial branches as well, such as ceramic and glass industry, polishing applications and gas sensing for carbon monoxide, *etc*., which makes it an industry-relevant material. Thanks to this large industrial interest, SnO_2 will never represent a bottleneck towards the commercialization of PSCs. From this point of view, organic layers and perovskite precursors require a more specific attention, than the SnO_2. Even as part of the TCO composition, such as ITO, SnO_2 represent only 10-20% of the total, and by far, is not the limiting factor compared to the availability of indium. The five locations with the highest concentration of cassiterite are reported in **Figure 12**.[195] For the production of metallic Sn (**Figure 12b**), China and Indonesia share the most significant part of the market, with 34% and 29% of the world production, respectively. According to Orlandi *et al.*, the demand for mineral Sn reaches about USD 6 billion/year with a current price set at USD 20/kg.[195]

For the potential commercialization of PSCs towards the terawatt scale, the manufacturing process must be extremely efficient. This directly reflects the need for a wise choice of the materials employed in the fabrication of PSCs. ESLs based on SnO_2 is a strong candidate to scale-up the perovskite technology since Sn is abundant and steadily available both in the oxide state and as a metallic precursor (**Figure 12c** and **d**). For the industrial manufacturing of PSCs,

SnO_2 can be deposited either from solutions or via physical vacuum deposition.[280] In the first case, slot-die coating of SnO_2 nanoparticles, sol-gel solutions, or colloidal dispersions are the preferred choice. The slot-die process is an already well-established coating technique in several industrial sectors, thanks to its high throughput and contained losses.[140] The concentration of SnO_2 in the slot-die inks is generally low in between 5%-15% w/v either in water or other green solvents. This is particularly important for the material cost (since SnO_2 consumption is low and the solvents are cheap) and for the process cost (since the deposition can be performed in air without specific requirements such as inert atmosphere, exotic safety protocols, *etc.* In the second case, SnO_2 can be deposited via RF magnetron sputtering starting from the sintered SnO_2 target.[280,281] Sputtering is a very common deposition technique in several industries, and even if the required capital expenditure (CAPEX) is higher than for slot-die coating (as well as its depreciation) it still represents a valid alternative. Towards large manufacturing, the main advantage of sputtering SnO_2 is represented by the simplicity of the target composition and its long shelf lifetime. On the contrary, ink formulations for slot-die coating may be affected by a shorter shelf life as well as potential IP protection strategies from the chemical companies, which may have negative effects on mass production.

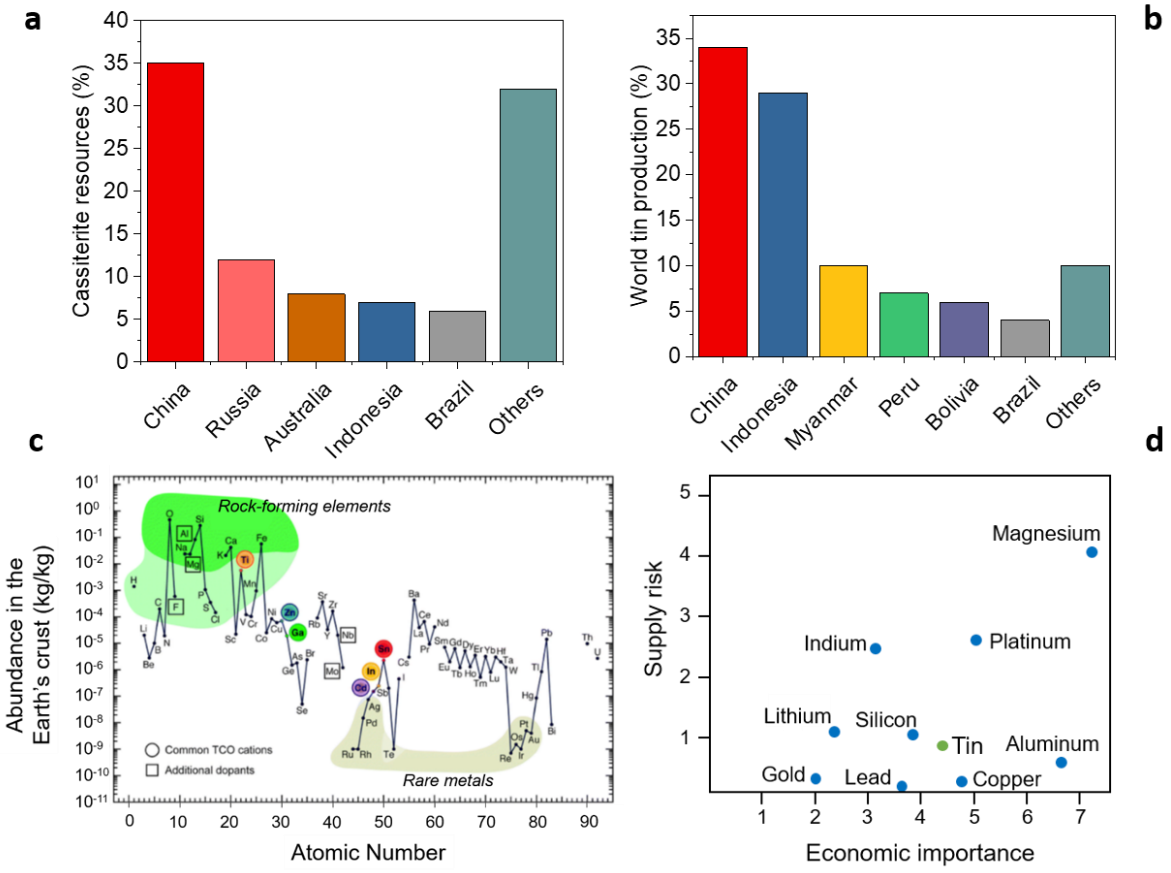

Figure 12. Resources of Sn a) on earth crust (as cassiterite) and b) mining production (between 2014 and 2018) for countries. (Data are collected from ref.[195]) c) Mass fraction abundance of the elements in the Earth's crust as a function of atomic number. Reproduced with permission.[282] Copyright 2011, The Royal Society of Chemistry. d) Supply risk and economic importance of some raw materials. (Panel d is replotted from ref. [195])

9. Toxicity-processing-safety relation of SnO_2 compounds

The potential mass usage of SnO_2 requires specific attention to its toxicity for the human health and environmental consequences. This topic needs to be discussed independently from the toxicity of the perovskite absorber and other layers. In general, the toxicological hazard associated with elemental Sn is mainly attributed to its heavy metal nature, resulting in similar environmental and health concerns caused by other much heavier metals such as mercury, cadmium, and lead.[283,284]

As discussed thoroughly in **Section 3**, organic and inorganic Sn compounds can be employed as precursor materials. Independent from the deposition technique, the routes of exposure to

these chemicals considered are through (i) gastrointestinal, (ii) dermal, and (iii) respiratory contact.[283,285,286] Through these main routes, humans and other organisms can be exposed to Sn and its compounds, but the extend of hazard that Sn can inflict is hereafter highly dependent on the chemical nature of its compound and its toxicokinetics.[283,285,287,288]. Here, we intentionally refrain from reporting based on single case studies that often present limitations in terms of significance, reproducibility, and choice of organism.

Due to their organic nature, organotin compounds such as TDMASn are readily and nearly entirely absorbed through all the above-mentioned routes.[283,285,289] Thereby, posing the highest health and environmental risks, it is important to note that its effects are lethal and carcinogenic in nature with a chronic oral minimal risk threshold level ranging up to 0.003mg/kg/day.[283,285,290,291] Fortunately, the usage of such compounds is limited to vacuum-based deposition, *e.g.,* TDMASn for ALD deposition, in which during normal circumstances, the organic precursor is only ever exposed inside the vacuum chamber. On the contrary, SnO and SnO_2, among other inorganic Sn compounds in this work, are largely naturally occurring and present limited toxicity.[283,285,292-294] However, as they are preferred in solution-based depositions, employing largely chlorinated Sn sources or the direct use of aqueous nanoparticle solutions, the probability of coming into contact with inorganic Sn compounds during processing is higher as compared more severe organotin compounds. In general, for inorganic Sn compounds, it has largely been concluded that the majority of compounds have low bioaccumulation, and are hence excreted shortly after uptake.[283,292-294] According to the last updated report of the U.S. Agency for Toxic Substances and Disease Registry (ATSDR), and based on comprehensive summaries of the World Health Organization (WHO) on heavy metals, no reports have been located detailing mortality as a result of exposure to inorganic Sn compounds.[283,285] In more detail, the general consensus holds that systematic chronic exposure to inorganic Sn compounds, such as dust or fumes, manifest a benign form of pneumoconiosis

that mainly involves the lower respiratory system.[295,296] Gastrointestinal effects have been recorded, such as nausea, vomiting, and diarrhea upon ingesting food items containing inorganic Sn, but these observations are based on numerous reports on chlorinated Sn-compounds.[297-299] Based on the available studies to date, no conclusive evidence is present to date supporting carcinogenic, reproductive, and developmental hurdles of inorganic Sn exposure aside from clear respiratory symptoms, hematological signs of anemia and gastrointestinal dissention. From there, it has been concluded that Sn being a heavy metal is found to mainly intercept vital metabolisms of other essential metals such as copper, zinc, and iron.[283,285,294] Therefore, in the case of both organic as well as inorganic Sn compounds, it is the disruption of the pharmacokinetics of these essential metals that is rather a at hand, and should be considered from a processing and manufacturing point of view. In the case of inorganic Sn compounds, a chronic oral minimal risk threshold level of 5 mg/kg/day has been determined.[283,285] Similar threshold values for its oxides remain unavailable at the time.

10. Summary and outlook

To summarize, SnO_2 has been intensively used in PSCs and demonstrated rapid progress owing to its attractive optical and electronic properties. Besides, the opportunity of processing at low temperatures with various techniques has accelerated the development of SnO_2 as ESL, which is attractive for large-scale deployment. In lab-scale devices, spin-cast SnO_2 ESLs prepared from colloidal nanoparticle dispersions have yielded up to a certified PCE of 23.52% (as of June 2020).

From a device perspective, SnO_2 provides much less parasitic absorption losses than other conventional ESLs, which enables high J_{SC} values (up to 24.9 mA/cm^2)[28] reported for SnO_2 ESLs-based PSCs. Such values are close the Shockley–Queisser (S-Q) limits (25.47 mA/cm^2 for 1.6 eV),[250] which implies that only marginal further improvements will be possible through

advanced optical device design. Although SnO_2-based PSCs lead to high V_{OC} values, V_{OC} losses (referencing the 1.23 V champion V_{OC} for a 1.6 eV bandgap perovskite)[164] of about the 79 meV (S-Q limit is 1.309 V for 1.60 eV)[250] offer still some room for advancements in terms of defect and contact passivation. Therefore, new and complementary (not only at the SnO_2/perovskite interface but also the grain boundaries and HTL/perovskite interfaces) passivation routes can be considered, as discussed in this review. Finally, new doping strategies may lead to decreased contact resistivities and improved *FF* values. Overall, advancing the PCE values beyond 25.2% seems a reasonable target when employing SnO_2 as ESL.

The PCE gap between the rigid (23.52%) and flexible PSCs (20.32%) is still significant. To close this gap, and bring roll-to-roll processed flexible solar cells to the market, more research efforts are needed, as well as thorough cost-lifetime analyses to decide which single-junction implementation has the highest chance to make it to the market.

Throughout this review, we attempted to provide an in-depth analysis of the highly efficient SnO_2 recipes, considering also scalability. In this regard, col-SnO_2 works efficiently for scalable solution-based techniques such as slot-die and spray coating. On the other hand, vacuum-based techniques such as sputtering and ALD offer advantages as well, but the amorphous nature of the low-temperature vacuum processed layers is a common handicap of these techniques and needs to be considered for the future development.

To date, most of the SnO_2-based modules have been fabricated at relatively small scale (<100 cm^2). However, for commercial viability, modules larger than 800 cm^2 (half of the typical silicon solar panels) need to be developed with competitive energy yields and operational stability as silicon PV technology. Considering the discussed scalable deposition techniques, it is not straightforward at present to point out one deposition technology for the required SnO_2 processing for such modules.

Finally, as the PV field is growing towards the tandem concept, utilization of the SnO_2 layer in tandem solar cells is also quite critical. The above-discussed advantages of SnO_2 make them directly integrable to mechanically stacked four-terminal (4-T) tandems since the top and bottom cells can be developed independently. In two-terminal (2-T) monolithic tandems, SnO_2 holds great potential for rough surfaces such as textured c-Si substrates with conformal deposition techniques such as sputtering and ALD. ALD SnO_2 is already successfully used as a buffer layer in tandem devices to protect the soft layers from the sputtering damage. As a future application, SnO_2 can be used as a recombination junction, which interconnects the top and bottom cells electronically, if the optoelectronic properties can be tuned for efficient tunneling recombination.

Supporting Information
Supporting Information is available from the Wiley Online Library.

Acknowledgment
This work was supported by the Scientific and Technical Research Council of Turkey (TUBITAK, Grant No. 119M149) and by the King Abdullah University of Science and Technology (KAUST) Office of Sponsored Research (OSR) under award No: OSR-2018-CARF/CCF-3079.

Conflict of Interest
The authors declare no conflıct of ınterest.

References

[1] A. Kojima, K. Teshima, Y. Shirai, T. Miyasaka, *J. Am. Chem. Soc.* **2009**, *131*, 6050.

[2] A. Mahapatra, D. Prochowicz, M. M. Tavakoli, S. Trivedi, P. Kumar, P. Yadav, *J. Mater. Chem. A* **2020**, *8*, 27.

[3] Y. Hou, E. Aydin, M. De Bastiani, C. Xiao, F. H. Isikgor, D.-J. Xue, B. Chen, H. Chen, B. Bahrami, A. H. Chowdhury, *Science* **2020**, *367*, 1135.

[4] S. De Wolf, J. Holovsky, S.-J. Moon, P. Löper, B. Niesen, M. Ledinsky, F.-J. Haug, J.-H. Yum, C. Ballif, *J. Phys. Chem. Lett.* **2014**, *5*, 1035.

[5] M. Ledinsky, T. Schönfeldová, J. Holovský, E. Aydin, Z. k. Hájková, L. Landová, N. Neyková, A. Fejfar, S. De Wolf, *J. Phys. Chem. Lett.* **2019**, *10*, 1368.

[6] Z. Yang, J. Dou, M. Wang, *Sol. RRL* **2018**, *2*, 1800177.

[7] A. Miyata, A. Mitioglu, P. Plochocka, O. Portugall, J. T. W. Wang, S. D. Stranks, H. J. Snaith, R. J. Nicholas, *Nat. Phys.* **2015**, *11*, 582.

[8] Z. Xiao, Z. Song, Y. Yan, *Adv. Mater.* **2019**, *31*, 1803792.

[9] W. J. Yin, T. Shi, Y. Yan, *Adv. Mater.* **2014**, *26*, 4653.

[10] B. Chen, S.-W. Baek, Y. Hou, E. Aydin, M. De Bastiani, B. Scheffel, A. Proppe, Z. Huang, M. Wei, Y.-K. Wang, *Nat. Commun.* **2020**, *11*, 1.

[11] S. Liu, Y. Guan, Y. Sheng, Y. Hu, Y. Rong, A. Mei, H. Han, *Adv. Energy Mater.* **2019**, *10*, 1902492.

[12] T. M. Brenner, D. A. Egger, L. Kronik, G. Hodes, D. Cahen, *Nat. Rev. Mater.* **2016**, *1*, 1.

[13] H.-S. Duan, H. Zhou, Q. Chen, P. Sun, S. Luo, T.-B. Song, B. Bob, Y. Yang, *Phys. Chem. Chem. Phys.* **2015**, *17*, 112.

[14] E. M. Hutter, G. E. Eperon, S. D. Stranks, T. J. Savenije, *J. Phys. Chem. Lett.* **2015**, *6*, 3082.

[15] G. Xing, N. Mathews, S. S. Lim, N. Yantara, X. Liu, D. Sabba, M. Grätzel, S. Mhaisalkar, T. C. Sum, *Nat. Mater.* **2014**, *13*, 476.

[16] N. G. Park, *Adv. Energy Mater.* **2020**, *10*, 1903106.

[17] W. Zhang, G. E. Eperon, H. J. Snaith, *Nat Energy* **2016**, *1*, 1.

[18] T.-B. Song, Q. Chen, H. Zhou, C. Jiang, H.-H. Wang, Y. M. Yang, Y. Liu, J. You, Y. Yang, *J. Mater. Chem. A* **2015**, *3*, 9032.

[19] *NREL Efficiency Chart* **2020**, *https://www.nrel.gov/pv/assets/pdfs/best-research-cell-efficiencies.20200406.pdf (accessed: June 2020).*

[20] B. Roose, Q. Wang, A. Abate, *Adv. Energy Mater.* **2019**, *9*, 1803140.

[21] K. Mahmood, S. Sarwar, M. T. Mehran, *RSC Adv.* **2017**, *7*, 17044.

[22] K. Wang, S. Olthof, W. S. Subhani, X. Jiang, Y. Cao, L. Duan, H. Wang, M. Du, S. F. Liu, *Nano Energy* **2019**, *68*, 104289.

[23] Z. K. Wang, L. S. Liao, *Adv. Opt. Mater.* **2018**, *6*, 1800276.

[24] D. Ouyang, Z. Huang, W. C. Choy, *Adv. Funct. Mater.* **2019**, *29*, 1804660.

[25] S. Sun, T. Buonassisi, J. P. Correa‐Baena, *Adv. Mater. Interfaces* **2018**, *5*, 1800408.

[26] Z. Huang, D. Ouyang, C. J. Shih, B. Yang, W. C. Choy, *Adv. Energy Mater.* **2019**, *10*, 1900903.

[27] W. Ke, G. Fang, Q. Liu, L. Xiong, P. Qin, H. Tao, J. Wang, H. Lei, B. Li, J. Wan, *J. Am. Chem. Soc.* **2015**, *137*, 6730.

[28] Q. Jiang, Y. Zhao, X. Zhang, X. Yang, Y. Chen, Z. Chu, Q. Ye, X. Li, Z. Yin, J. You, *Nat. Photonics* **2019**, *13*, 460.

[29] P. Zhao, Z. Lin, J. Wang, M. Yue, J. Su, J. Zhang, J. Chang, Y. Hao, *ACS Appl. Energy Mater.* **2019**, *2*, 4504.

[30] H. Yi, D. Wang, M. A. Mahmud, F. Haque, M. B. Upama, C. Xu, L. Duan, A. Uddin, *ACS Appl. Energy Mater.* **2018**, *1*, 6027.

[31] M. Ulfa, P. Wang, J. Zhang, J. Liu, W. D. de Marcillac, L. Coolen, S. b. Peralta, T. Pauporté, *ACS Appl. Mater. Interfaces* **2018**, *10*, 35118.

[32] H. S. Rao, B. X. Chen, W. G. Li, Y. F. Xu, H. Y. Chen, D. B. Kuang, C. Y. Su, *Adv. Funct. Mater.* **2015**, *25*, 7200.

[33] L. Huang, X. Sun, C. Li, J. Xu, R. Xu, Y. Du, J. Ni, H. Cai, J. Li, Z. Hu, *ACS Appl. Mater. Interfaces* **2017**, *9*, 21909.

[34] Y. Bai, Y. Fang, Y. Deng, Q. Wang, J. Zhao, X. Zheng, Y. Zhang, J. Huang, *ChemSusChem* **2016**, *9*, 2686.

[35] Q. Jiang, X. Zhang, J. You, *Small* **2018**, *14*, 1801154.

[36] K. Huang, Y. Peng, Y. Gao, J. Shi, H. Li, X. Mo, H. Huang, Y. Gao, L. Ding, J. Yang, *Adv. Energy Mater.* **2019**, *9*, 1901419.

[37] D. Liu, Y. Wang, H. Xu, H. Zheng, T. Zhang, P. Zhang, F. Wang, J. Wu, Z. Wang, Z. Chen, *Sol. RRL* **2019**, *3*, 1800292.

[38] P. Tiwana, P. Docampo, M. B. Johnston, H. J. Snaith, L. M. Herz, *ACS Nano* **2011**, *5*, 5158.

[39] J. Song, E. Zheng, J. Bian, X.-F. Wang, W. Tian, Y. Sanehira, T. Miyasaka, *J. Mater. Chem. A* **2015**, *3*, 10837.

[40] C. Gong, S. Tong, K. Huang, H. Li, H. Huang, J. Zhang, J. Yang, *Sol. RRL* **2020**, *4*, 1900204.

[41] T. Bu, J. Li, F. Zheng, W. Chen, X. Wen, Z. Ku, Y. Peng, J. Zhong, Y.-B. Cheng, F. Huang, *Nat. Commun.* **2018**, *9*, 1.

[42] Y. Y. Kim, T. Y. Yang, R. Suhonen, M. Välimäki, T. Maaninen, A. Kemppainen, N. J. Jeon, J. Seo, *Adv. Sci.* **2019**, *6*, 1802094.

[43] Q. Wali, Y. Iqbal, B. Pal, A. Lowe, R. Jose, *Sol. Energy Mater. Sol. Cells* **2018**, *179*, 102.

[44] G. Yang, P. Qin, G. Fang, G. Li, *J. Energy Chem.* **2018**, *27*, 962.

[45] L. Xiong, Y. Guo, J. Wen, H. Liu, G. Yang, P. Qin, G. Fang, *Adv. Funct. Mater.* **2018**, *28*, 1802757.

[46] M. Zhang, X. Zhan, *Adv. Energy Mater.* **2019**, *9*, 1900860.

[47] A. A. Said, J. Xie, Q. Zhang, *Small* **2019**, *15*, 1900854.

[48] X. Ren, Z. S. Wang, W. C. Choy, *Adv. Opt. Mater.* **2019**, *7*, 1900407.

[49] F. Wang, Y. Cao, C. Chen, Q. Chen, X. Wu, X. Li, T. Qin, W. Huang, *Adv. Funct. Mater.* **2018**, *28*, 1803753.

[50] U. Würfel, A. Cuevas, P. Würfel, *IEEE J. Photovoltaics* **2014**, *5*, 461.

[51] J. K. Katahara, H. W. Hillhouse, *J. Appl. Phys* **2014**, *116*, 173504.

[52] M. Stolterfoht, P. Caprioglio, C. M. Wolff, J. A. Márquez, J. Nordmann, S. Zhang, D. Rothhardt, U. Hörmann, Y. Amir, A. Redinger, *Energy Environ. Sci.* **2019**, *12*, 2778.

[53] E. H. Anaraki, A. Kermanpur, L. Steier, K. Domanski, T. Matsui, W. Tress, M. Saliba, A. Abate, M. Grätzel, A. Hagfeldt, J.-P. Correa-Baena, *Energy Environ. Sci.* **2016**, *9*, 3128.

[54] S. Gharibzadeh, B. Abdollahi Nejand, M. Jakoby, T. Abzieher, D. Hauschild, S. Moghadamzadeh, J. A. Schwenzer, P. Brenner, R. Schmager, A. A. Haghighirad, *Adv. Energy Mater.* **2019**, *9*, 1803699.

[55] J. Peng, J. I. Khan, W. Liu, E. Ugur, T. Duong, Y. Wu, H. Shen, K. Wang, H. Dang, E. Aydin, *Adv. Energy Mater.* **2018**, *8*, 1801208.

[56] J. Peng, Y. Wu, W. Ye, D. A. Jacobs, H. Shen, X. Fu, Y. Wan, N. Wu, C. Barugkin, H. T. Nguyen, *Energy Environ. Sci.* **2017**, *10*, 1792.

[57] M. Stolterfoht, C. M. Wolff, J. A. Márquez, S. Zhang, C. J. Hages, D. Rothhardt, S. Albrecht, P. L. Burn, P. Meredith, T. Unold, *Nat Energy* **2018**, *3*, 847.

[58] M. F. M. Noh, C. H. Teh, R. Daik, E. L. Lim, C. C. Yap, M. A. Ibrahim, N. A. Ludin, A. R. bin Mohd Yusoff, J. Jang, M. A. M. Teridi, *J. Mater. Chem. C* **2018**, *6*, 682.

[59] Q. Liu, M. C. Qin, W. J. Ke, X. L. Zheng, Z. Chen, P. L. Qin, L. B. Xiong, H. W. Lei, J. W. Wan, J. Wen, *Adv. Funct. Mater.* **2016**, *26*, 6069.

[60] M. Saliba, T. Matsui, J. Y. Seo, K. Domanski, J. P. Correa-Baena, M. K. Nazeeruddin, S. M. Zakeeruddin, W. Tress, A. Abate, A. Hagfeldt, M. Gratzel, *Energy Environ. Sci.* **2016**, *9*, 1989.

[61] L. Lin, Z. Yang, E. Jiang, Z. Wang, J. Yan, N. Li, Z. Wang, Y. Ai, C. Shou, B. Yan, *ACS Appl. Energy Mater.* **2019**, *2*, 7062.

[62] U. Thakur, P. Kumar, S. Gusarov, A. E. Kobryn, S. Riddell, A. Goswami, K. Alam, S. Savela, P. Kar, T. Thundat, *ACS Appl. Mater. Interfaces* **2020**.

[63] C. Zuo, L. Ding, *Adv. Energy Mater.* **2017**, *7*, 1601193.

[64] C. Momblona, L. Gil-Escrig, E. Bandiello, E. M. Hutter, M. Sessolo, K. Lederer, J. Blochwitz-Nimoth, H. J. Bolink, *Energy Environ. Sci.* **2016**, *9*, 3456.

[65] M. Morales‐Masis, S. De Wolf, R. Woods‐Robinson, J. W. Ager, C. Ballif, *Adv. Electron. Mater.* **2017**, *3*, 1600529.

[66] H. R. Tan, A. Jain, O. Voznyy, X. Z. Lan, F. P. G. de Arquer, J. Z. Fan, R. Quintero-Bermudez, M. J. Yuan, B. Zhang, Y. C. Zhao, F. J. Fan, P. C. Li, L. N. Quan, Y. B. Zhao, Z. H. Lu, Z. Y. Yang, S. Hoogland, E. H. Sargent, *Science* **2017**, *355*, 722.

[67] J. J. Choi, X. H. Yang, Z. M. Norman, S. J. L. Billinge, J. S. Owen, *Nano Lett.* **2014**, *14*, 127.

[68] S. Mohamed, *J. Alloys Compd.* **2012**, *510*, 119.

[69] A. F. Khan, M. Mehmood, M. Aslam, M. Ashraf, *Appl. Surf. Sci.* **2010**, *256*, 2252.

[70] X. Shi, R. Chen, T. Jiang, S. Ma, X. Liu, Y. Ding, M. Cai, J. Wu, S. Dai, *Sol. RRL* **2019**, *4*, 1900198.

[71] D. Wang, S.-C. Chen, Q. Zheng, *J. Mater. Chem. C* **2019**, *7*, 12204.

[72] K. H. Sun, *J. Am. Ceram. Soc.* **1947**, *30*, 282.

[73] E. Çetinörgü, S. Goldsmith, Y. Rosenberg, R. Boxman, *J. Non. Cryst. Solids* **2007**, *353*, 2595.

[74] Ç. Kılıç, A. Zunger, *Phys. Rev. Lett.* **2002**, *88*, 095501.

[75] H. J. Snaith, A. Abate, J. M. Ball, G. E. Eperon, T. Leijtens, N. K. Noel, S. D. Stranks, J. T.-W. Wang, K. Wojciechowski, W. Zhang, *J. Phys. Chem. Lett.* **2014**, *5*, 1511.

[76] J. P. C. Baena, L. Steier, W. Tress, M. Saliba, S. Neutzner, T. Matsui, F. Giordano, T. J. Jacobsson, A. R. S. Kandada, S. M. Zakeeruddin, *Energy Environ. Sci.* **2015**, *8*, 2928.

[77] M. De Bastiani, E. Aydin, T. Allen, D. Walter, A. Fell, J. Peng, N. Gasparini, J. Troughton, D. Baran, K. Weber, *Adv. Electron. Mater.* **2019**, *5*, 1800500.

[78] E. Aydin, M. De Bastiani, S. De Wolf, *Adv. Mater.* **2019**, *31*, 1900428.

[79] W. Ke, D. Zhao, A. J. Cimaroli, C. R. Grice, P. Qin, Q. Liu, L. Xiong, Y. Yan, G. Fang, *J. Mater. Chem. A* **2015**, *3*, 24163.

[80] M. Zhu, W. Liu, W. Ke, L. Xie, P. Dong, F. Hao, *ACS Appl. Mater. Interfaces* **2018**, *11*, 666.

[81] H. Shan, E. Rezaee, X. Leng, X. Wang, Q. Chen, Z. X. Xu, *ChemSusChem* **2018**, *11*, 3000.

[82] T. Leijtens, G. E. Eperon, S. Pathak, A. Abate, M. M. Lee, H. J. Snaith, *Nat. Commun.* **2013**, *4*, 1.

[83] S. Ito, S. Tanaka, K. Manabe, H. Nishino, *J. Phys. Chem. C* **2014**, *118*, 16995.

[84] X. Guo, H. Dong, W. Li, N. Li, L. Wang, *ChemPhysChem* **2015**, *16*, 1727.

[85] R. C. Liu, F. L. Liang, W. Zhou, Y. S. Yang, Z. H. Zhu, *Nano Energy* **2015**, *12*, 115.

[86] T. Singh, J. Singh, T. Miyasaka, *ChemSusChem* **2016**, *9*, 2559.

[87] J. Yang, B. D. Siempelkamp, E. Mosconi, F. De Angelis, T. L. Kelly, *Chem. Mater.* **2015**, *27*, 4229.

[88] C. Wang, D. Zhao, C. R. Grice, W. Liao, Y. Yu, A. Cimaroli, N. Shrestha, P. J. Roland, J. Chen, Z. Yu, *J. Mater. Chem. A* **2016**, *4*, 12080.

[89] B. Roose, J. P. C. Baena, K. C. Godel, M. Graetzel, A. Hagfeldt, U. Steiner, A. Abate, *Nano Energy* **2016**, *30*, 517.

[90] J. A. Christians, P. Schulz, J. S. Tinkham, T. H. Schloemer, S. P. Harvey, B. J. T. de Villers, A. Sellinger, J. J. Berry, J. M. Luther, *Nat Energy* **2018**, *3*, 68.

[91] B. Roose, C. M. Johansen, K. Dupraz, T. Jaouen, P. Aebi, U. Steiner, A. Abate, *J. Mater. Chem. A* **2018**, *6*, 1850.

[92] Q. S. Dong, Y. T. Shi, C. Y. Zhang, Y. K. Wu, L. D. Wang, *Nano Energy* **2017**, *40*, 336.

[93] M. Neophytou, M. De Bastiani, N. Gasparini, E. Aydin, E. Ugur, A. Seitkhan, F. Moruzzi, Y. Choaie, A. J. Ramadan, J. R. Troughton, *ACS Appl. Energy Mater.* **2019**, *2*, 8090.

[94] G. Bai, Z. Wu, J. Li, T. Bu, W. Li, W. Li, F. Huang, Q. Zhang, Y.-B. Cheng, J. Zhong, *Sol. Energy* **2019**, *183*, 306.

[95] L. Xiong, M. Qin, G. Yang, Y. Guo, H. Lei, Q. Liu, W. Ke, H. Tao, P. Qin, S. Li, *J. Mater. Chem. A* **2016**, *4*, 8374.

[96] H. S. Jung, G. S. Han, N.-G. Park, M. J. Ko, *Joule* **2019**, *3*, 1850.

[97] T. Leijtens, K. A. Bush, R. Prasanna, M. D. McGehee, *Nat Energy* **2018**, *3*, 828.

[98] S. Albrecht, M. Saliba, J. P. C. Baena, F. Lang, L. Kegelmann, M. Mews, L. Steier, A. Abate, J. Rappich, L. Korte, *Energy Environ. Sci.* **2016**, *9*, 81.

[99] T. Liu, K. Chen, Q. Hu, R. Zhu, Q. Gong, *Adv. Energy Mater.* **2016**, *6*, 1600457.

[100] J. Y. Jeng, Y. F. Chiang, M. H. Lee, S. R. Peng, T. F. Guo, P. Chen, T. C. Wen, *Adv. Mater.* **2013**, *25*, 3727.

[101] G. Yu, J. Gao, J. C. Hummelen, F. Wudl, A. J. Heeger, *Science* **1995**, *270*, 1789.

[102] T. Bu, S. Shi, J. Li, Y. Liu, J. Shi, L. Chen, X. Liu, J. Qiu, Z. Ku, Y. Peng, *ACS Appl. Mater. Interfaces* **2018**, *10*, 14922.

[103] N. Wang, K. Zhao, T. Ding, W. Liu, A. S. Ahmed, Z. Wang, M. Tian, X. W. Sun, Q. Zhang, *Adv. Energy Mater.* **2017**, *7*, 1700522.

[104] K. Wang, M. C. Tang, H. X. Dang, R. Munir, D. Barrit, M. De Bastiani, E. Aydin, D. M. Smilgies, S. De Wolf, A. Amassian, *Adv. Mater.* **2019**, *31*, 1808357.

[105] H. X. Dang, K. Wang, M. Ghasemi, M.-C. Tang, M. De Bastiani, E. Aydin, E. Dauzon, D. Barrit, J. Peng, D.-M. Smilgies, *Joule* **2019**, *3*, 1746.

[106] R. Wang, M. Mujahid, Y. Duan, Z. K. Wang, J. Xue, Y. Yang, *Adv. Funct. Mater.* **2019**, *29*, 1808843.

[107] J. Bovatsek, A. Tamhankar, R. Patel, N. Bulgakova, J. Bonse, *Thin Solid Films* **2010**, *518*, 2897.

[108] S. S. Shin, S. J. Lee, S. I. Seok, *Adv. Funct. Mater.* **2019**, *29*, 1900455.

[109] M. C. Sellers, E. G. Seebauer, *Thin Solid Films* **2011**, *519*, 2103.

[110] S. Y. Park, M. Y. Baek, Y. Ju, D. H. Kim, C. S. Moon, J. H. Noh, H. S. Jung, *J. Phys. Chem. Lett.* **2018**, *9*, 5460.

[111] Z. Song, W. Bi, X. Zhuang, Y. Wu, B. Zhang, X. Chen, C. Chen, Q. Dai, H. Song, *Sol. RRL* **2019**, *4*, 1900266.

[112] R. Li, Y. Zhou, M. Sun, Z. Gong, Y. Guo, F. Wu, W. Li, W. Ding, *Coatings* **2019**, *9*, 591.

[113] G. Yang, C. Chen, F. Yao, Z. Chen, Q. Zhang, X. Zheng, J. Ma, H. Lei, P. Qin, L. Xiong, *Adv. Mater.* **2018**, *30*, 1706023.

[114] P. Zhang, J. Wu, T. Zhang, Y. Wang, D. Liu, H. Chen, L. Ji, C. Liu, W. Ahmad, Z. D. Chen, *Adv. Mater.* **2018**, *30*, 1703737.

[115] N. A. Jayah, H. Yahaya, M. R. Mahmood, T. Terasako, K. Yasui, A. M. Hashim, *Nanoscale Res. Lett.* **2015**, *10*, 1.

[116] C. Maragliano, S. Lilliu, M. Dahlem, M. Chiesa, T. Souier, M. Stefancich, *Sci. Rep.* **2014**, *4*, 4203.

[117] S. Yang, X. Song, L. Gao, N. Wang, X. Ding, S. Wang, T. Ma, *ACS Appl. Energy Mater.* **2018**, *1*, 4564.

[118] Y. Guo, J. Tao, F. Shi, X. Hu, Z. Hu, K. Zhang, W. Cheng, S. Zuo, J. Jiang, J. Chu, *ACS Appl. Energy Mater.* **2018**, *1*, 2000.

[119] X. F. Ling, J. Y. Yuan, D. A. Liu, Y. J. Wang, Y. N. Zhang, S. Chen, H. H. Wu, F. Jin, F. P. Wu, G. Z. Shi, X. Tang, J. W. Zheng, S. Z. Liu, Z. K. Liu, W. L. Ma, *ACS Appl. Mater. Interfaces* **2017**, *9*, 23181.

[120] Y. Zhou, X. Li, H. Lin, *Small* **2019**, *16*, 1902579.

[121] N. Tsvetkov, B. C. Moon, J. Y. Lee, J. K. Kang, *ACS Appl. Energy Mater.* **2019**, *3*, 344.

[122] C. Wang, Y. Tang, Y. Hu, L. Huang, J. Fu, J. Jin, W. Shi, L. Wang, W. Yang, *RSC Adv.* **2015**, *5*, 52041.

[123] O. Tufte, P. Chapman, *Phys. Rev.* **1967**, *155*, 796.

[124] S. Wu, R. Chen, S. Zhang, B. H. Babu, Y. Yue, H. Zhu, Z. Yang, C. Chen, W. Chen, Y. Huang, *Nat. Commun.* **2019**, *10*, 1.

[125] P. W. Liang, C. C. Chueh, S. T. Williams, A. K. Y. Jen, *Adv. Energy Mater.* **2015**, *5*, 1402321.

[126] V. Balderrama, J. Sanchez, M. Estrada, J. Ferre-Borrull, J. Pallares, L. F. Marsal, *IEEE J. Photovoltaics* **2015**, *5*, 1093.

[127] K. Hoshimono, S. Fujimori, S. Fujita, S. Fujita, *Jpn. J. Appl. Phys.* **1993**, *32*, L1070.

[128] Z. Li, T. R. Klein, D. H. Kim, M. Yang, J. J. Berry, M. F. van Hest, K. Zhu, *Nat. Rev. Mater.* **2018**, *3*, 1.

[129] D. H. Kim, J. B. Whitaker, Z. Li, M. F. van Hest, K. Zhu, *Joule* **2018**, *2*, 1437.

[130] N.-G. Park, K. Zhu, *Nat. Rev. Mater.* **2020**, *5*, 1.

[131] L. Huang, X. X. Sun, C. Li, J. Xu, R. Xu, Y. Y. Du, J. Ni, H. K. Cai, J. Li, Z. Y. Hu, J. J. Jianjun, *ACS Appl. Mater. Interfaces* **2017**, *9*, 21909.

[132] L. J. Zuo, H. X. Guo, D. W. deQuilettes, S. Jariwala, N. De Marco, S. Q. Dong, R. DeBlock, D. S. Ginger, B. Dunn, M. K. Wang, Y. Yang, *Sci. Adv.* **2017**, *3*.

[133] H. B. Lee, M. K. Jeon, N. Kumar, B. Tyagi, J. W. Kang, *Adv. Funct. Mater.* **2019**, *29*, 1903213.

[134] A. S. Subbiah, N. Mathews, S. Mhaisalkar, S. K. Sarkar, *ACS Energy Lett.* **2018**, *3*, 1482.

[135] J. Li, H. Wang, X. Y. Chin, H. A. Dewi, K. Vergeer, T. W. Goh, J. W. M. Lim, J. H. Lew, K. P. Loh, C. Soci, *Joule* **2020**, *4*.

[136] Q. Jiang, L. Zhang, H. Wang, X. Yang, J. Meng, H. Liu, Z. Yin, J. Wu, X. Zhang, J. You, *Nat Energy* **2016**, *2*, 1.

[137] G. S. Han, J. Kim, S. Bae, S. Han, Y. J. Kim, O. Y. Gong, P. Lee, M. J. Ko, H. S. Jung, *ACS Energy Lett.* **2019**, *4*, 1845.

[138] Z. Liu, L. Qiu, L. K. Ono, S. He, Z. Hu, M. Jiang, G. Tong, Z. Wu, Y. Jiang, D.-Y. Son, *Nat Energy* **2020**, 1.

[139] J. Zhang, W. Zhang, H.-M. Cheng, S. R. P. Silva, *Mater. Today* **2020**.

[140] J. B. Whitaker, D. H. Kim, B. W. Larson, F. Zhang, J. J. Berry, M. F. van Hest, K. Zhu, *Sustain. Energy Fuels* **2018**, *2*, 2442.

[141] F. Di Giacomo, S. Shanmugam, H. Fledderus, B. J. Bruijnaers, W. J. Verhees, M. S. Dorenkamper, S. C. Veenstra, W. Qiu, R. Gehlhaar, T. Merckx, *Sol. Energy Mater. Sol. Cells* **2018**, *181*, 53.

[142] L. Gao, K. Huang, C. Long, F. Zeng, B. Liu, J. Yang, *Appl. Phys. A* **2020**, *126*, 452.

[143] F. Di Giacomo, H. Fledderus, H. Gorter, G. Kirchner, I. de Vries, I. Dogan, W. Verhees, V. Zardetto, M. Najafi, D. Zhang, presented at *WCPEC*, Hawai, June, **2018**.

[144] Y. Deng, E. Peng, Y. Shao, Z. Xiao, Q. Dong, J. Huang, *Energy Environ. Sci.* **2015**, *8*, 1544.

[145] Y. Deng, X. Zheng, Y. Bai, Q. Wang, J. Zhao, J. Huang, *Nat Energy* **2018**, *3*, 560.

[146] Y. Peng, F. Zeng, Y. Cheng, C. Wang, K. Huang, P. Xie, H. Xie, Y. Gao, J. Yang, *Org. Electron.* **2020**, *83*, 105736.

[147] B. Dou, J. B. Whitaker, K. Bruening, D. T. Moore, L. M. Wheeler, J. Ryter, N. J. Breslin, J. J. Berry, S. M. Garner, F. S. Barnes, S. E. Shaheen, C. J. Tassone, K. Zhu, M. F. van Hest, *ACS Energy Lett.* **2018**, *3*, 2558.

[148] S. Sansoni, M. De Bastiani, E. Aydin, E. Ugur, F. H. Isikgor, A. Al‐Zahrani, F. Lamberti, F. Laquai, M. Meneghetti, S. De Wolf, *Adv. Mater. Technol.* **2020**, *5*, 1901009.

[149] J. W. Lee, D. K. Lee, D. N. Jeong, N. G. Park, *Adv. Funct. Mater.* **2019**, *29*, 1807047.

[150] C. Liu, Y.-B. Cheng, Z. Ge, *Chem. Soc. Rev.* **2020**, *49*, 1653.

[151] J. E. Bishop, T. J. Routledge, D. G. Lidzey, *J. Phys. Chem. Lett.* **2018**, *9*, 1977.

[152] J. A. Smith, O. S. Game, J. E. Bishop, E. Spooner, R. C. Kilbride, C. Greenland, R. Jayaprakash, T. Alanazi, E. J. Cassella, A. Tejada, *ACS Appl. Energy Mater.* **2020**, *3*.

[153] A. A. Abdul-Hamead, *AIP Conf. Proc.* **2018**, *1968*, 030017.

[154] K. Derrar, M. Zaabat, I. Zerrouk, A. Hafdallah, N. Rouabah, B. Gasmi, *Defect Diffus. Forum* **2019**, *397*, 179.

[155] S. Choudhury, S. Gunjal, N. Kumari, K. Diwate, K. Mohite, A. Bhattacharjee, *Mater. Today Proc.* **2016**, *3*, 1609.

[156] V.-H. Tran, R. B. Ambade, S. B. Ambade, S.-H. Lee, I.-H. Lee, *ACS Appl. Mater. Interfaces* **2017**, *9*, 1645.

[157] S. Ebrahimiasl, A. Zakaria, *Sensors* **2014**, *14*, 2549.

[158] J. Jang, H. Yim, Y. H. Cho, D. H. Kang, J. W. Choi, *센서학회지* **2015**, *24*, 364.

[159] M. Li, W. W. Zuo, Q. Wang, K. L. Wang, M. P. Zhuo, H. Köbler, C. E. Halbig, S. Eigler, Y. G. Yang, X. Y. Gao, *Adv. Energy Mater.* **2019**, *10*, 1902653.

[160] M. M. Tavakoli, P. Yadav, D. Prochowicz, M. Sponseller, A. Osherov, V. Bulović, J. Kong, *Adv. Energy Mater.* **2019**, *9*, 1803587.

[161] T. Bu, X. Liu, Y. Zhou, J. Yi, X. Huang, L. Luo, J. Xiao, Z. Ku, Y. Peng, F. Huang, *Energy Environ. Sci.* **2017**, *10*, 2509.

[162] S. Seo, S. Jeong, H. Park, H. Shin, N.-G. Park, *Chem. Commun.* **2019**, *55*, 2403.

[163] D. Muñoz-Rojas, T. Maindron, A. Esteve, F. Piallat, J. Kools, J.-M. Decams, *Mater. Today Chem.* **2019**, *12*, 96.

[164] J.-P. Correa-Baena, W. Tress, K. Domanski, E. H. Anaraki, S.-H. Turren-Cruz, B. Roose, P. P. Boix, M. Grätzel, M. Saliba, A. Abate, *Energy Environ. Sci.* **2017**, *10*, 1207.

[165] Y. Lee, S. Lee, G. Seo, S. Paek, K. T. Cho, A. J. Huckaba, M. Calizzi, D. w. Choi, J. S. Park, D. Lee, *Adv. Sci.* **2018**, *5*, 1800130.

[166] S. Jeong, S. Seo, H. Park, H. Shin, *Chem. Commun.* **2019**, *55*, 2433.

[167] J. Li, T. Bu, Y. Liu, J. Zhou, J. Shi, Z. Ku, Y. Peng, J. Zhong, Y. B. Cheng, F. Huang, *ChemSusChem* **2018**, *11*, 2898.

[168] Y. Mo, J. Shi, P. Zhou, S. Li, T. Bu, Y.-B. Cheng, F. Huang, *Sol. RRL* **2019**, *3*, 1900209.

[169] M. Kam, Q. Zhang, D. Zhang, Z. Fan, *Sci. Rep.* **2019**, *9*, 1.

[170] E. Aydin, J. Troughton, M. De Bastiani, E. Ugur, M. Sajjad, A. Alzahrani, M. Neophytou, U. Schwingenschlögl, F. Laquai, D. Baran, *ACS Appl. Energy Mater.* **2018**, *1*, 6227.

[171] L. Qiu, Z. Liu, L. K. Ono, Y. Jiang, D. Y. Son, Z. Hawash, S. He, Y. Qi, *Adv. Funct. Mater.* **2018**, *29*, 1806779.

[172] Y. Porte, R. Maller, H. Faber, H. N. AlShareef, T. D. Anthopoulos, M. A. McLachlan, *J. Mater. Chem. C* **2016**, *4*, 758.

[173] M. El Khakani, R. Dolbec, A. Serventi, M. Horrillo, M. Trudeau, R. Saint-Jacques, D. Rickerby, I. Sayago, *Sens. Actuator B-Chem.* **2001**, *77*, 383.

[174] Z. Chen, G. Yang, X. Zheng, H. Lei, C. Chen, J. Ma, H. Wang, G. Fang, *J. Power Sources* **2017**, *351*, 123.

[175] V. M. Kiyek, Y. A. Birkhölzer, Y. Smirnov, M. Ledinsky, Z. Remes, J. Momand, B. J. Kooi, G. Koster, G. Rijnders, M. Morales‐Masis, *Adv. Mater. Interfaces* **2020**, *7*, 2000162.

[176] N. Abdullah, N. Ismail, D. Nuruzzaman, *IOP Conf. Ser. Mater. Sci. Eng* **2018**, *319*, 012022.

[177] S. K. Tripathy, V. Rajeswari, *AIP Conf. Proc.* **2014**, *1576*, 176.

[178] Y. Guo, X. Yin, J. Liu, W. Chen, S. Wen, M. Que, H. Xie, Y. Yang, W. Que, B. Gao, *Org. Electron.* **2019**, *65*, 207.

[179] J. Ma, X. Zheng, H. Lei, W. Ke, C. Chen, Z. Chen, G. Yang, G. Fang, *Sol. RRL* **2017**, *1*, 1700118.

[180] H. Sun, Y. Zhou, Y. Xin, K. Deng, L. Meng, J. Xiong, L. Li, *Adv. Funct. Mater.* **2019**, *29*, 1808667.

[181] A. Chilvery, S. Das, P. Guggilla, C. Brantley, A. Sunda-Meya, *Sci. Technol. Adv. Mater.* **2016**, *17*, 650.

[182] L. Zuo, H. Guo, D. W. deQuilettes, S. Jariwala, N. De Marco, S. Dong, R. DeBlock, D. S. Ginger, B. Dunn, M. Wang, *Sci. Adv.* **2017**, *3*, e1700106.

[183] C. Chen, Y. Jiang, J. Guo, X. Wu, W. Zhang, S. Wu, X. Gao, X. Hu, Q. Wang, G. Zhou, *Adv. Funct. Mater.* **2019**, *29*, 1900557.

[184] Q. Dong, J. Li, Y. Shi, M. Chen, L. K. Ono, K. Zhou, C. Zhang, Y. Qi, Y. Zhou, N. P. Padture, *Adv. Energy Mater.* **2019**, *9*, 1900834.

[185] S.-H. Turren-Cruz, A. Hagfeldt, M. Saliba, *Science* **2018**, *362*, 449.

[186] C. Wang, C. Xiao, Y. Yu, D. Zhao, R. A. Awni, C. R. Grice, K. Ghimire, I. Constantinou, W. Liao, A. J. Cimaroli, *Adv. Energy Mater.* **2017**, *7*, 1700414.

[187] L. Qiu, S. He, Y. Jiang, D.-Y. Son, L. K. Ono, Z. Liu, T. Kim, T. Bouloumis, S. Kazaoui, Y. Qi, *J. Mater. Chem. A* **2019**, *7*, 6920.

[188] B. Taheri, E. Calabrò, F. Matteocci, D. Di Girolamo, G. Cardone, A. Liscio, A. Di Carlo, F. Brunetti, *Energy Technol.* **2020**, 1901284.

[189] L. Luo, Y. Zhang, N. Chai, X. Deng, J. Zhong, F. Huang, Y. Peng, Z. Ku, Y.-B. Cheng, *J. Mater. Chem. A* **2018**, *6*, 21143.

[190] E. Calabrò, F. Matteocci, A. L. Palma, L. Vesce, B. Taheri, L. Carlini, I. Pis, S. Nappini, J. Dagar, C. Battocchio, *Sol. Energy Mater. Sol. Cells* **2018**, *185*, 136.

[191] S. Das, V. Jayaraman, *Prog. Mater. Sci.* **2014**, *66*, 112.

[192] L. Gracia, A. Beltrán, J. Andrés, *J. Phys. Chem. B* **2007**, *111*, 6479.

[193] A. Alsac, A. Yildiz, T. Serin, N. Serin, *J. Appl. Phys.* **2013**, *113*, 063701.

[194] H. Kawazoe, K. Ueda, *J. Am. Ceram. Soc.* **1999**, *82*, 3330.

[195] M. O. Orlandi, *Tin Oxide Materials: Synthesis, Properties, and Applications*, Elsevier, Amsterdam, Netherlands **2019**.

[196] K. G. Godinho, A. Walsh, G. W. Watson, *J. Phys. Chem. C* **2009**, *113*, 439.

[197] N. K. Noel, S. N. Habisreutinger, B. Wenger, Y. H. Lin, F. Zhang, J. B. Patel, A. Kahn, M. B. Johnston, H. J. Snaith, *Adv. Energy Mater.* **2020**, *10*, 1903231.

[198] Z. Yang, B. H. Babu, S. Wu, T. Liu, S. Fang, Z. Xiong, L. Han, W. Chen, *Sol. RRL* **2019**, *4*, 1900257.

[199] Z. Zhou, S. Pang, Z. Liu, H. Xu, G. Cui, *J. Mater. Chem. A* **2015**, *3*, 19205.

[200] M. Park, J.-Y. Kim, H. J. Son, C.-H. Lee, S. S. Jang, M. J. Ko, *Nano Energy* **2016**, *26*, 208.

[201] E. Wang, P. Chen, X. Yin, Y. Wu, W. Que, *Sol. RRL* **2019**, *3*, 1900041.

[202] J. Tian, J. Zhang, X. Li, B. Cheng, J. Yu, W. Ho, *Sol. RRL* **2020**, *4*, 2000090.

[203] Y. W. Noh, J. H. Lee, I. S. Jin, S. H. Park, J. W. Jung, *Nano Energy* **2019**, *65*, 104014.

[204] E. Halvani Anaraki, A. Kermanpur, M. T. Mayer, L. Steier, T. Ahmed, S.-H. Turren-Cruz, J. Seo, J. Luo, S. M. Zakeeruddin, W. R. Tress, *ACS Energy Lett.* **2018**, *3*, 773.

[205] J. Song, W. Zhang, D. Wang, K. Deng, J. Wu, Z. Lan, *Sol. Energy* **2019**, *185*, 508.

[206] S. Akin, *ACS Appl. Mater. Interfaces* **2019**, *11*, 39998.

[207] R. D. Shannon, *Acta Crystallogr. Sec. A* **1976**, *32*, 751.

[208] K. Choi, J. Lee, H. I. Kim, C. W. Park, G.-W. Kim, H. Choi, S. Park, S. A. Park, T. Park, *Energy Environ. Sci.* **2018**, *11*, 3238.

[209] P. Zhu, S. Gu, X. Luo, Y. Gao, S. Li, J. Zhu, H. Tan, *Adv. Energy Mater.* **2019**, *10*, 1903083.

[210] Z. Liu, K. Deng, J. Hu, L. Li, *Angew. Chem.* **2019**, *131*, 11621.

[211] J. Liang, Z. Chen, G. Yang, H. Wang, F. Ye, C. Tao, G. Fang, *ACS Appl. Mater. Interfaces* **2019**, *11*, 23152.

[212] W. Chen, Y. Zhou, G. Chen, Y. Wu, B. Tu, F. Z. Liu, L. Huang, A. M. C. Ng, A. B. Djurišić, Z. He, *Adv. Energy Mater.* **2019**, *9*, 1803872.

[213] M. Abdi-Jalebi, Z. Andaji-Garmaroudi, S. Cacovich, C. Stavrakas, B. Philippe, J. M. Richter, M. Alsari, E. P. Booker, E. M. Hutter, A. J. Pearson, *Nature* **2018**, *555*, 497.

[214] X. Liu, Y. Zhang, L. Shi, Z. Liu, J. Huang, J. S. Yun, Y. Zeng, A. Pu, K. Sun, Z. Hameiri, *Adv. Energy Mater.* **2018**, *8*, 1800138.

[215] C. Huang, P. Lin, N. Fu, K. Sun, M. Ye, C. Liu, X. Zhou, L. Shu, X. Hao, B. Xu, *J. Mater. Chem. A* **2018**, *6*, 22086.

[216] N. K. Noel, S. N. Habisreutinger, B. Wenger, Y. H. Lin, F. Zhang, J. B. Patel, A. Kahn, M. B. Johnston, H. J. Snaith, *Adv. Energy Mater.* **2019**, *10*, 1903231.

[217] V. Ferguson, S. R. P. Silva, W. Zhang, *Energy Environ. Mater.* **2019**, *2*, 107.

[218] S. Wang, Y. Zhu, B. Liu, C. Wang, R. Ma, *J. Mater. Chem. A* **2019**, *7*, 5353.

[219] W. Hui, Y. Yang, Q. Xu, H. Gu, S. Feng, Z. Su, M. Zhang, J. Wang, X. Li, J. Fang, *Adv. Mater.* **2019**, *32*, 1906374.

[220] H. Tang, Q. Cao, Z. He, S. Wang, J. Han, T. Li, B. Gao, J. Yang, D. Deng, X. Li, *Sol. RRL* **2020**, *4*, 1900415.

[221] S. P. Pujari, L. Scheres, A. T. Marcelis, H. Zuilhof, *Angew. Chem. Int. Ed.* **2014**, *53*, 6322.

[222] A. Mingorance, H. Xie, H. S. Kim, Z. Wang, M. Balsells, A. Morales‐Melgares, N. Domingo, N. Kazuteru, W. Tress, J. Fraxedas, *Adv. Mater. Interfaces* **2018**, *5*, 1800367.

[223] X. Zhang, Z. Shi, H. Lu, X. Li, H. Wang, S. Yuan, F. Liu, Y. Pan, Z. Weng, H. Zhang, *J. Mater. Chem. A* **2019**, *7*, 22323.

[224] D. Yang, R. Yang, K. Wang, C. Wu, X. Zhu, J. Feng, X. Ren, G. Fang, S. Priya, S. F. Liu, *Nat. Commun.* **2018**, *9*, 3239.

[225] J. Chen, X. Zhao, S. G. Kim, N. G. Park, *Adv. Mater.* **2019**, *31*, 1902902.

[226] E. Jiang, Y. Ai, J. Yan, N. Li, L. Lin, Z. Wang, C. Shou, B. Yan, Y. Zeng, J. Sheng, *ACS Appl. Mater. Interfaces* **2019**, *11*, 36727.

[227] L. J. Zuo, Q. Chen, N. De Marco, Y. T. Hsieh, H. J. Chen, P. Y. Sun, S. Y. Chang, H. X. Zhao, S. Q. Dong, Y. Yang, *Nano Lett.* **2017**, *17*, 269.

[228] M. Hou, H. Zhang, Z. Wang, Y. Xia, Y. Chen, W. Huang, *ACS Appl. Mater. Interfaces* **2018**, *10*, 30607.

[229] H.-L. Yip, A. K.-Y. Jen, *Energy Environ. Sci.* **2012**, *5*, 5994.

[230] G. Yang, C. Wang, H. Lei, X. Zheng, P. Qin, L. Xiong, X. Zhao, Y. Yan, G. Fang, *J. Mater. Chem. A* **2017**, *5*, 1658.

[231] S. K. Hau, Y.-J. Cheng, H.-L. Yip, Y. Zhang, H. Ma, A. K.-Y. Jen, *ACS Appl. Mater. Interfaces* **2010**, *2*, 1892.

[232] M. Liu, Z. Chen, Z. Chen, H.-L. Yip, Y. Cao, *Mater. Chem. Front.* **2019**, *3*, 496.

[233] B. Tu, Y. Shao, W. Chen, Y. Wu, X. Li, Y. He, J. Li, F. Liu, Z. Zhang, Y. Lin, *Adv. Mater.* **2019**, *31*, 1805944.

[234] K. Liu, S. Chen, J. Wu, H. Zhang, M. Qin, X. Lu, Y. Tu, Q. Meng, X. Zhan, *Energy Environ. Sci.* **2018**, *11*, 3463.

[235] T. Cao, K. Chen, Q. Chen, Y. Zhou, N. Chen, Y. Li, *ACS Appl. Mater. Interfaces* **2019**, *11*, 33825.

[236] C. Tian, K. Lin, J. Lu, W. Feng, P. Song, L. Xie, Z. Wei, *Small Methods* **2019**, *4*, 1900476.

[237] Y. Zhou, C. Fuentes-Hernandez, J. Shim, J. Meyer, A. J. Giordano, H. Li, P. Winget, T. Papadopoulos, H. Cheun, J. Kim, *Science* **2012**, *336*, 327.

[238] H. P. Zhou, Q. Chen, G. Li, S. Luo, T. B. Song, H. S. Duan, Z. R. Hong, J. B. You, Y. S. Liu, Y. Yang, *Science* **2014**, *345*, 542.

[239] H. Zhang, H. Azimi, Y. Hou, T. Ameri, T. Przybilla, E. Spiecker, M. Kraft, U. Scherf, C. J. Brabec, *Chem. Mater.* **2014**, *26*, 5190.

[240] X. Huang, J. Du, X. Guo, Z. Lin, J. Ma, J. Su, L. Feng, C. Zhang, J. Zhang, J. Chang, *Sol. RRL* **2019**, *4*, 1900336.

[241] J. Wei, F. Guo, X. Wang, K. Xu, M. Lei, Y. Liang, Y. Zhao, D. Xu, *Adv. Mater.* **2018**, *30*, 1805153.

[242] J. Wu, Y. Cui, B. Yu, K. Liu, Y. Li, H. Li, J. Shi, H. Wu, Y. Luo, D. Li, *Adv. Funct. Mater.* **2019**, *29*, 1905336.

[243] P. Qin, T. Wu, Z. Wang, X. Zheng, X. Yu, G. Fang, G. Li, *Sol. RRL* **2019**, *3*, 1900134.

[244] Y. Ai, W. Liu, C. Shou, J. Yan, N. Li, Z. Yang, W. Song, B. Yan, J. Sheng, J. Ye, *Sol. Energy* **2019**, *194*, 541.

[245] Y. Luan, X. Yi, P. Mao, Y. Wei, J. Zhuang, N. Chen, T. Lin, C. Li, J. Wang, *iScience* **2019**, *16*, 433.

[246] J. Xie, K. Huang, X. Yu, Z. Yang, K. Xiao, Y. Qiang, X. Zhu, L. Xu, P. Wang, C. Cui, *Acs Nano* **2017**, *11*, 9176.

[247] H. Dong, L. Zhang, J. Li, J. Fuhao, B. Jiao, X. Hou, J. Liu, Z. Wu, *J. Mater. Chem. A* **2020**, *8*.

[248] J. Du, L. Feng, X. Guo, X. Huang, Z. Lin, J. Su, Z. Hu, J. Zhang, J. Chang, Y. Hao, *J. Power Sources* **2020**, *455*, 227974.

[249] H. Xia, X. Li, J. Zhou, B. Wang, Y. Chu, Y. Li, G. Wu, D. Zhang, B. Xue, X. Zhang, *ACS Appl. Energy Mater.* **2020**, *3*, 3186.

[250] S. Rühle, *Sol. Energy* **2016**, *130*, 139.

[251] S. S. Mali, J. V. Patil, H. Arandiyan, C. K. Hong, *J. Mater. Chem. A* **2019**, *7*, 17516.

[252] G. Martínez-Denegri, S. Colodrero, M. Kramarenko, J. Martorell, *ACS Appl. Energy Mater.* **2018**, *1*, 5548.

[253] Q. Cao, Z. Li, J. Han, S. Wang, J. Zhu, H. Tang, X. Li, X. Li, *Sol. RRL* **2019**, *3*, 1900333.

[254] M. Hu, L. Zhang, S. She, J. Wu, X. Zhou, X. Li, D. Wang, J. Miao, G. Mi, H. Chen, *Sol. RRL* **2019**, *4*, 1900331.

[255] P. Huang, Q. Chen, K. Zhang, L. Yuan, Y. Zhou, B. Song, Y. Li, *J. Mater. Chem. A* **2019**, *7*, 6213.

[256] F. Wang, Y. Zhang, M. Yang, J. Du, L. Xue, L. Yang, L. Fan, Y. Sui, J. Yang, X. Zhang, *Nano Energy* **2019**, *63*, 103825.

[257] Y. Gao, Y. Wu, Y. Liu, C. Chen, X. Shen, X. Bai, Z. Shi, W. W. Yu, Q. Dai, Y. Zhang, *Sol. RRL* **2019**, *3*, 1900314.

[258] P. Wang, R. Li, B. Chen, F. Hou, J. Zhang, Y. Zhao, X. Zhang, *Adv. Mater.* **2020**, *32*, 1905766.

[259] N. Arora, M. I. Dar, S. Akin, R. Uchida, T. Baumeler, Y. Liu, S. M. Zakeeruddin, M. Grätzel, *Small* **2019**, *15*, 1904746.

[260] M. Singh, A. Ng, Z. Ren, H. Hu, H.-C. Lin, C.-W. Chu, G. Li, *Nano Energy* **2019**, *60*, 275.

[261] Q. Sun, H. Li, X. Gong, H. Ban, Y. Shen, M. Wang, *Sol. RRL* **2019**, *4*, 1900229.

[262] C. Liu, L. Zhang, X. Zhou, J. Gao, W. Chen, X. Wang, B. Xu, *Adv. Funct. Mater.* **2019**, *29*, 1807604.

[263] F. Di Giacomo, A. Fakharuddin, R. Jose, T. M. Brown, *Energy Environ. Sci.* **2016**, *9*, 3007.

[264] S. Shi, J. Li, T. Bu, S. Yang, J. Xiao, Y. Peng, W. Li, J. Zhong, Z. Ku, Y.-B. Cheng, *RSC Adv.* **2019**, *9*, 9946.

[265] D. Xin, Z. Wang, M. Zhang, X. Zheng, Y. Qin, J. Zhu, W.-H. Zhang, *ACS Sustain. Chem. Eng.* **2019**, *7*, 4343.

[266] J. W. Elam, D. A. Baker, A. J. Hryn, A. B. Martinson, M. J. Pellin, J. T. Hupp, *J. Vac. Sci. Technol.* **2008**, *26*, 244.

[267] C. Wang, L. Guan, D. Zhao, Y. Yu, C. R. Grice, Z. Song, R. A. Awni, J. Chen, J. Wang, X. Zhao, *ACS Energy Lett.* **2017**, *2*, 2118.

[268] N. Zhu, X. Qi, Y. Zhang, G. Liu, C. Wu, D. Wang, X. Guo, W. Luo, X. Li, H. Hu, *ACS Appl. Energy Mater.* **2019**, *2*, 3676.

[269] G. Ouyang, X. Li, X. Tan, G. Yang, *Appl. Phys. Lett.* **2006**, *89*, 031904.

[270] W. J. Lee, A. J. Clancy, E. Kontturi, A. Bismarck, M. S. Shaffer, *ACS Appl. Mater. Interfaces* **2016**, *8*, 31500.

[271] M. V. Khenkin, E. A. Katz, A. Abate, G. Bardizza, J. J. Berry, C. Brabec, F. Brunetti, V. Bulović, Q. Burlingame, A. Di Carlo, *Nat Energy* **2020**, *5*, 35.

[272] M. Jošt, L. Kegelmann, L. Korte, S. Albrecht, *Adv. Energy Mater.* **2020**, 1904102.

[273] K. A. Bush, C. D. Bailie, Y. Chen, A. R. Bowring, W. Wang, W. Ma, T. Leijtens, F. Moghadam, M. D. McGehee, *Adv. Mater.* **2016**, *28*, 3937.

[274] M. Morales-Masis, S. M. De Nicolas, J. Holovsky, S. De Wolf, C. Ballif, *IEEE J. Photovoltaics* **2015**, *5*, 1340.

[275] E. Aydin, M. De Bastiani, X. Yang, M. Sajjad, F. Aljamaan, Y. Smirnov, M. N. Hedhili, W. Liu, T. G. Allen, L. Xu, *Adv. Funct. Mater.* **2019**, *29*, 1901741.

[276] M. Schultes, T. Helder, E. Ahlswede, M. F. Aygüler, P. Jackson, S. Paetel, J. A. Schwenzer, I. M. Hossain, U. W. Paetzold, M. Powalla, *ACS Appl. Energy Mater.* **2019**, *2*, 7823.

[277] J. Xu, C. C. Boyd, J. Y. Zhengshan, A. F. Palmstrom, D. J. Witter, B. W. Larson, R. M. France, J. Werner, S. P. Harvey, E. J. Wolf, *Science* **2020**, *367*, 1097.

[278] F. Sahli, J. Werner, B. A. Kamino, M. Bräuninger, R. Monnard, B. Paviet-Salomon, L. Barraud, L. Ding, J. J. D. Leon, D. Sacchetto, *Nat. Mater.* **2018**, *17*, 820.

[279] E. Wiberg, N. Wiberg, A. F. Holleman, *Inorganic Chemistry*, Academic Press, San Diego, USA **2001**.

[280] Z. Song, C. L. McElvany, A. B. Phillips, I. Celik, P. W. Krantz, S. C. Watthage, G. K. Liyanage, D. Apul, M. J. Heben, *Energy Environ. Sci.* **2017**, *10*, 1297.

[281] J. Xiao, *PhD Thesis*, Massachusetts Institute of Technology, June, **2018**.

[282] R. M. Pasquarelli, D. S. Ginley, R. O'Hayre, *Chem. Soc. Rev.* **2011**, *40*, 5406.

[283] C. Harper, *Toxicological profile for tin and tin compounds*, United States Agency for Toxic Substances and Disease Registry, Atlanta, GA, USA **2005**.

[284] HSDB, *Tin: Environmental standards and regulations*, National Library of Medicine, Hazardous Substances databank, Bethesda, MD **2003**.

[285] WHO, *WHO Food Additives Series 46:TIN* World Health Organization, Geneva, Switzerland **2003**.

[286] EPA, Environmental Protection Agency, Office of Research and Development, Cincinnati, OH: U.S **1987**.

[287] NIOSH, *NIOSH pocket guide to chemical hazards.Tin*, National Institute for Occupational Safety and Health, Washington, DC **2003**.

[288] J. M. Stellman, *Encyclopaedia of occupational health and safety*, International Labour Organization, Geneva, Switzerland **1998**.

[289] WHO, *Tin and Organotin Compounds: A Preliminary Review-Environmental Health Criteria 15*, World Health Organization, Geneva, Switzerland **1980**.

[290] WHO, *International programme on chemical safety. Environmental health criteria 116: Tributyltin compounds*, World Health Organization, Geneva, Switzerland **1990**.

[291] WHO, *Concise International Chemical Assessment Document 13: Triphenyltin compounds*, World Health Organization, Geneva, Switzerland **1999**.

[292] NIOSH/OSHA, *Occupational health guideline for inorganic tin compounds. Occupational Health Guidelines for Chemical Hazards.* , National Institute for Occupational Safety and Health/Occupational Safety and Health Administration Washington, DC **1981**.

[293] NIOSH, National Institute for Occupational Safety and Health., Washington, DC **2003**.

[294] ICRP, *Metabolic data for tin*, International Commission on Radiological Protection., **1981**

[295] IPCS, *International Chemical Safety Card- Tin (IV) oxide*, World Health Organisation, International Programme on Chemical Safety (ICSC 0954), Geneva, Switzerland **2004**.

[296] IPCS, *International Chemical Safety Card- Tin (II) oxide*, World Health Organisation, International Programme on Chemical Safety (ICSC 0956), Geneva, Switzerland **2004**.

[297] IPCS, *International Chemical Safety Card- Tin (II) chloride dehydrate*, World Health Organisation, International Programme on Chemical Safety (ICSC 0738), Geneva, Switzerland **2004**.

[298] IPCS, *International Chemical Safety Card- Tin (II) chloride anhydrous*, World Health Organisation, International Programme on Chemical Safety (ICSC 0955), Geneva, Switzerland **2004**.

[299] IPCS, *International Chemical Safety Card- Tin (IV) chloride anhydrous.* , World Health Organisation, International Programme on Chemical Safety (ICSC 0953), Geneva, Switzerland **2004**.